Baroclinic Instability and the Summer Southern Hemisphere Wavenumber 5 Circulation

by Agnes Chi-Man Chan

A thesis submitted to the Faculty of Graduate Studies and Research in partial fulfillment of the requirements for the degree of Master of Science.

December, 1987

Department of Meteorology

McGill University

Montreal, Quebec, Canada

Short-Title...

Summer-S-Hemisphere Wavenumber-5 Circulation

ABSTRACT

We examine the linear instability of the observed two-dimensional (latitude/height) January 1979 zonal wind of the mid-latitude Southern Hemisphere. The model used is a 10-level, linear, quasi-geostrophic 45°S β-plane channel model, with 30 Fourier harmonics in the meridional direction and a single harmonic in the zonal direction. The most unstable mode has a zonal wavelength corresponding to wavenumber 12 at 45°S. The mode corresponding to zonal wavenumber 5 at 45°S is also baroclinically unstable. Its latitude-height structure bears qualitative resemblance to the observed wavenumber 5 circulation, which frequently dominates the summer Southern Hemisphere mid-latitude circulation. The latitude of the maximum eddy amplitude at 50°S is simulated, but the maximum is located near the surface instead of aloft. Effects of surface dissipation and a normalization of the zonal wind by the cosine of latitude are also considered.

RÉSUMÉ

Nous examinons l'instabilité linéaire du vent longitudinal bi-dimensionnel (latitude/hauteur) en janvier 1979 dans les latitudes moyennes de l'hémisphère sud. Nous utilisons un modèle linéaire, quasi-géostrophe sur plan β à 45°S. Celui-ci possède 10 niveaux verticaux, 30 harmoniques de surface méridionnales et une seule harmonique longitudinale. Le mode le plus instable a une longeur d'onde correspondant au nombre d'onde longitudinal 12 à 45°S. Le mode qui correspond au nombre d'onde longitudinal 5 à 45°S est de plus baroclinement instable. Sa structure en latitude/hauteur ressemble qualitativement à celle du nombre d'onde 5 dérivée des observations. Nous obtenons bien un maximum d'amplitudes des perturbation à 50°S mais celui-ci est situé près de la surface plutôt qu'en hauteur. Les effets de la dissipation de surface et d'une normalisation du vent longitudinal par le cosinus de la latitude sont également considérés.

Acknowledgements

I wish to express my deepest gratitude to my thesis supervisor, Dr. C.A. Lin for his invaluable advice, patient guidance and indispensable support throughout my studies.

I am grateful to the Natural Sciences and Engineering Research Council, and the Atmospheric Environment Service for the financial support of this study. I wish to thank Dr. S. Lambert of the Canadian Climate Centre, Atmospheric Environment Service, for providing the observed data needed for this project.

I also would like to thank Ms. Ann Cossette for typing the thesis, and Ms. Ursula Seidenfuss for drafting the figures.

Last but not least, I would like to thank my family for all the support and understanding they have given me throughout my studies. As a token of my appreciation I wish to dedicate this thesis to them.

TABLE OF CONTENTS

List of Figures

CHAPTER 1

Introduction

Medium scale waves, consisting largely of zonal wavenumbers 4-7, frequently dominate the Southern Hemisphere summer circulation pattern. Salby (1982) noted predominant wavenumber 5 patterns are frequently found in the temperature fields of the lower stratosphere, during the summer months of FGGE. These pentagonal features appear to remain quasi-stationary or propagate eastward with periods of about 10 days. The eastward phase progression and wave structure in the vertical are consistent with features of a baroclinic instability, with a sharp scale selection mechanism in both time and space. Hamilton (1983), using a data set of the Australian Bureau of Meteorology, also noted a prominent wavenumber 5 peak in the geopotential height zonal wavenumber spectra of the 300- and 500-mb surfaces in the Southern Hemisphere summer. Similar findings were also reported by Randel and Stanford (1983), in an analysis of National Meteorological Center (NMC) geopotential height fields for the 1978-79 summer. They suggested that the waves might be maintained by the zonal mean kinetic energy. In subsequent observational studies (Randel and Stanford, 1985a, 1985b, 1985c), the same authors found that the vacillations in the wave-zonal mean exchange, with a time scale of 10-20 days, result from nonlinear baroclinic instability, and identified well-defined life cycles of baroclinic growth, maturity and barotropic decay. Interference between the baroclinic eastward moving waves and quasi-stationary medium scale waves was also observed. A specific case of the life cycle of the baroclinic instability was examined by Randel and Stanford (1985c) using zonally averaged diagnostics.

Lambert (1986) examined the eddy kinetic energy (EKE) budget of the winter and summer Southern Hemisphere circulations during 1979. The data set used was the FGGE analyses of the European Centre for Medium Range Weather Forecasts. The terms evaluated as a function of zonal wavenumber (m) were EKE, conversion C(EAPE,EKE) of eddy available potential energy (EAPE) to EKE, conversion C(EKE,ZKE) of EKE to zonal kinetic energy (ZKE), the transfer of EKE among waves by nonlinear interaction (L), and the boundary flux (LB) of EKE. The results for January 1979 are shown in Fig. 1.1. We see there is a prominent peak in wave kinetic energy at wavenumber 5; the dominant terms in the budget equation are the conversion of EAPE to EKE, and EKE to ZKE, and probably dissipation. This suggests that the wave 5 circulation is due to a baroclinic instability. This maximum of EKE at zonal wavenumber 5 occurs at about latitude 45°S.

Chen et al. (1986) also analyzed the same data set and showed that the medium scale waves (zonal wavenumbers 4-6) contribute about half of the total eddy transport of momentum and sensible heat in the Southern Hemisphere summer general circulation. The developing stages of these waves are dominated by baroclinic processes and the decay stage by barotropic processes. They thus suggested that the waves are a manifestation of classic baroclinic instability.

Charney (1947) and Eady (1949) first demonstrated that baroclinically unstable waves could grow on a mean zonal wind with vertical shear. The fastest growing mode has zonal length scales of about 5000 km and is maintained by the release of available potential energy of the mean state. Brown (1969a,b) extended the instability analysis using a basic flow with both vertical and lateral shears using an initial value approach. He identified unstable modes with sources of energy being the zonal

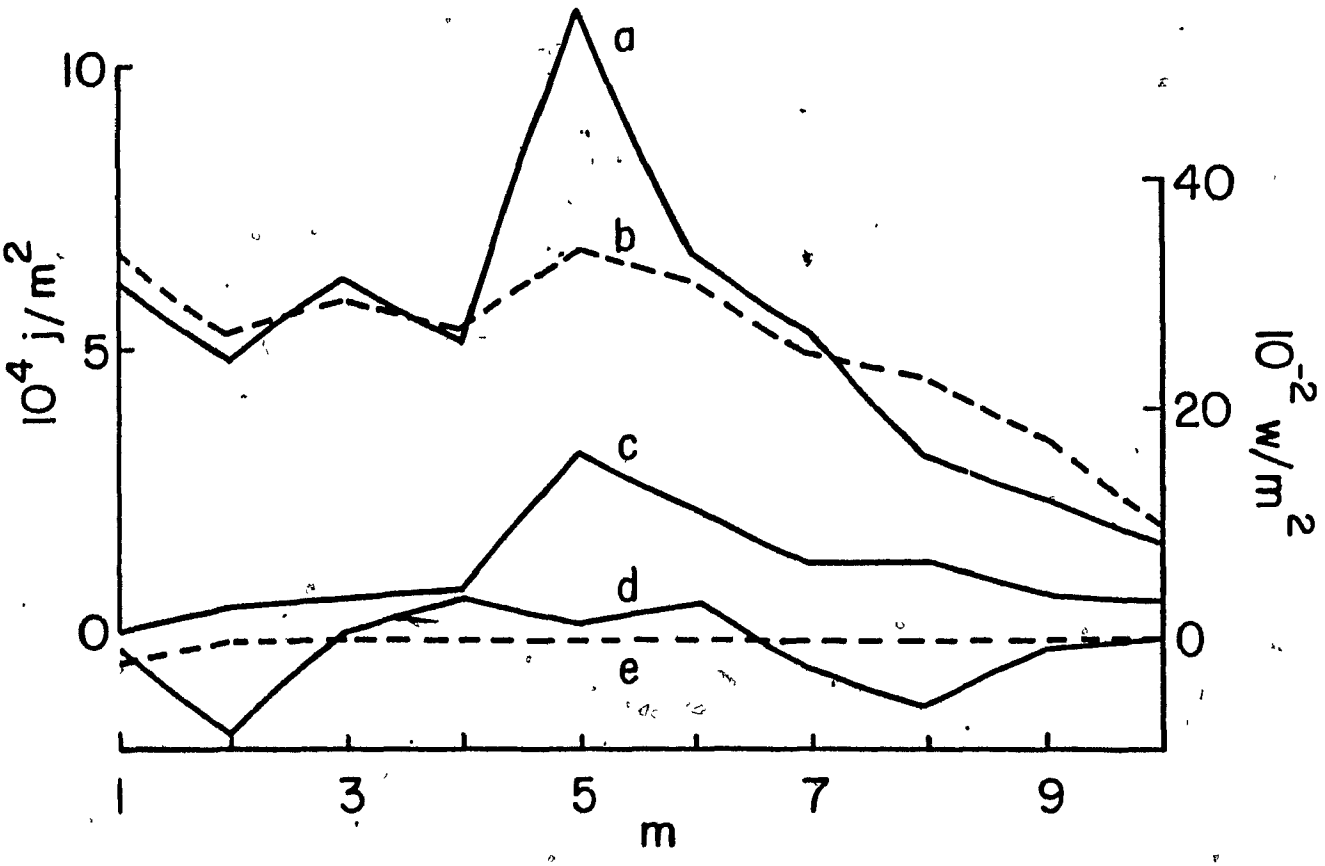

Figure 1.1 Terms of the eddy kinetic budget as a function of zonal wavenumber(m). The curves labelled a, b, c, d, e describe the terms EKE. C(EAPE, EKE), C(EKE, ZKE), L, LB respectively. The scale on the left applies to EKE, while the one on the right applies to the other quantities (adapted from Lambert, 1986).

available potential energy or the zonal kinetic energy. Song (1971a,b) examined the instability properties of similar basic states, using an eigenvalue technique. Unstable modes with energy sources associated with the vertical and horizontal shears were found. All these studies used the quasi-geostrophic equations on a β-plane. Later studies by Gall (1976) have used the primitive equations with spherical geometry and an initial value approach to investigate the linear instability of two-dimensional zonal mean flows. He found that for the zonal wavenumber range 1-15, the fastest growing modes are wavenumbers 12-15. However, the wavenumbers that dominate the intermediate scale transient eddies in a general circulation model are longer (wavenumbers 5-7). In addition, the linear theory predicts maximum perturbation amplitude for wavenumbers 5-7 to be near the earth's surface, while the maximum amplitude for waves of similar scale in the general circulation model are located in the upper troposphere. Gall attributed these discrepencies to nonlinear effects. Frederiksen (1981a) examined the instability characteristics of observed Southern Hemisphere zonally averaged flows using a linear spherical, quasi-geostrophic model. He used an eigenvalue technique and identified different families of unstable modes. The appropriate unstable modes do have maximum streamfunction amplitude and eddy fluxes at the correct latitudes, but the amplitudes of the streamfunction, momentum and heat fluxes are also too large at the surface when compared to observations. He found that for one basic state, the second fastest growing mode, and not the mode with the largest growth rate, corresponds most closely with observations. Frederiksen made no specific attempt to identify the wavenumber 5 disturbance. Kalnay and Mo (1986) performed mechanistic experiments with a general circulation model to determine the origin of Southern Hemisphere

stationary Rossby waves. In their "easterly deceleration" experiment, where the initial zonal flow is decelerated by adding a negative solid body rotation velocity of 5 m/s at the equator, a pentagonal stationary wave structure is generated. They suggested that this phenomenon might be related to the observed wavenumber 5 in the Southern Hemisphere summer.

In this study, we use a 10-level linear quasi-geostrophic β-plane model to investigate the baroclinic instability of an observed two-dimensional Southern Hemisphere mean zonal flow, that of January 1979. The wind and temperature data for the latter are taken from Lambert's (1986) data set. An eigenvalue technique is used, which yields unstable modes in addition to the one with the fastest growth rate. The perturbation structures are compared to observations of the wavenumber 5 circulation during 1979 obtained from Lambert's data set. The results will show whether linear baroclinic instability of the observed zonal mean flow can account for the wavenumber 5 circulation. This is of great interest as some of the observational studies already referred to strongly suggest that baroclinic instability is a plausible mechanism for the maintenance of these waves.

CHAPTER 2

The Model and the Basic State

A. Formulation of the model

We use a 10-level, quasi-geostrophic mid-latitude β-plane model. The horizontal and vertical scales of the wavenumber 5 disturbance are such that quasi-geostrophic dynamics is expected to give good results. The motion takes place in a cyclic zonal channel with channel walls at $y=0$ and $y=\pi L$ in the meridional (y) direction, and of length $2\pi L$ in the zonal (x) direction. The Coriolis parameter $f = f_o + \beta y$ is assumed to have a constant meridional gradient β; f_o and β are evaluated at 45^oS. The distance πL is identified as the latitudinal extent of 50^o latitude, from 20^oS to 70^oS. In the vertical direction, the model atmosphere is divided into ten layers of equal mass, from 0 to 100 mb, 100-200 mb, ---, 900-1000 mb, with flat top and bottom boundaries. Pressure is used as the vertical coordinate. Quantities with subscripts 0, 2, 4, ---, 20 denote values at the full pressure levels 0, 100, 200, ---, 1000 mb respectively; odd values of the subscript indicate the half pressure levels 50, 150, ---, 950 mb. The model geometry in the vertical is shown in Fig. 2.1.

The governing quasi-geostrophic equations describe physically the conservation of potential vorticity. Mathematically, these may be written as

$$\frac{d_k}{dt} q_k = 0 \qquad k = 1, 3, 5, ---, 19 \qquad (1)$$

where

$$\frac{d}{dt} = \frac{\partial}{\partial t} + u_k \frac{\partial}{\partial x} + v_k \frac{\partial}{\partial y}$$

$$u_k = -\frac{\partial \psi_k}{\partial y} \qquad v_k = \frac{\partial \psi_k}{\partial x}$$

$$q_1 = \left(\nabla^2 - \mu_2^2\right) \psi_1 + \mu_2^2 \psi_3 + f$$

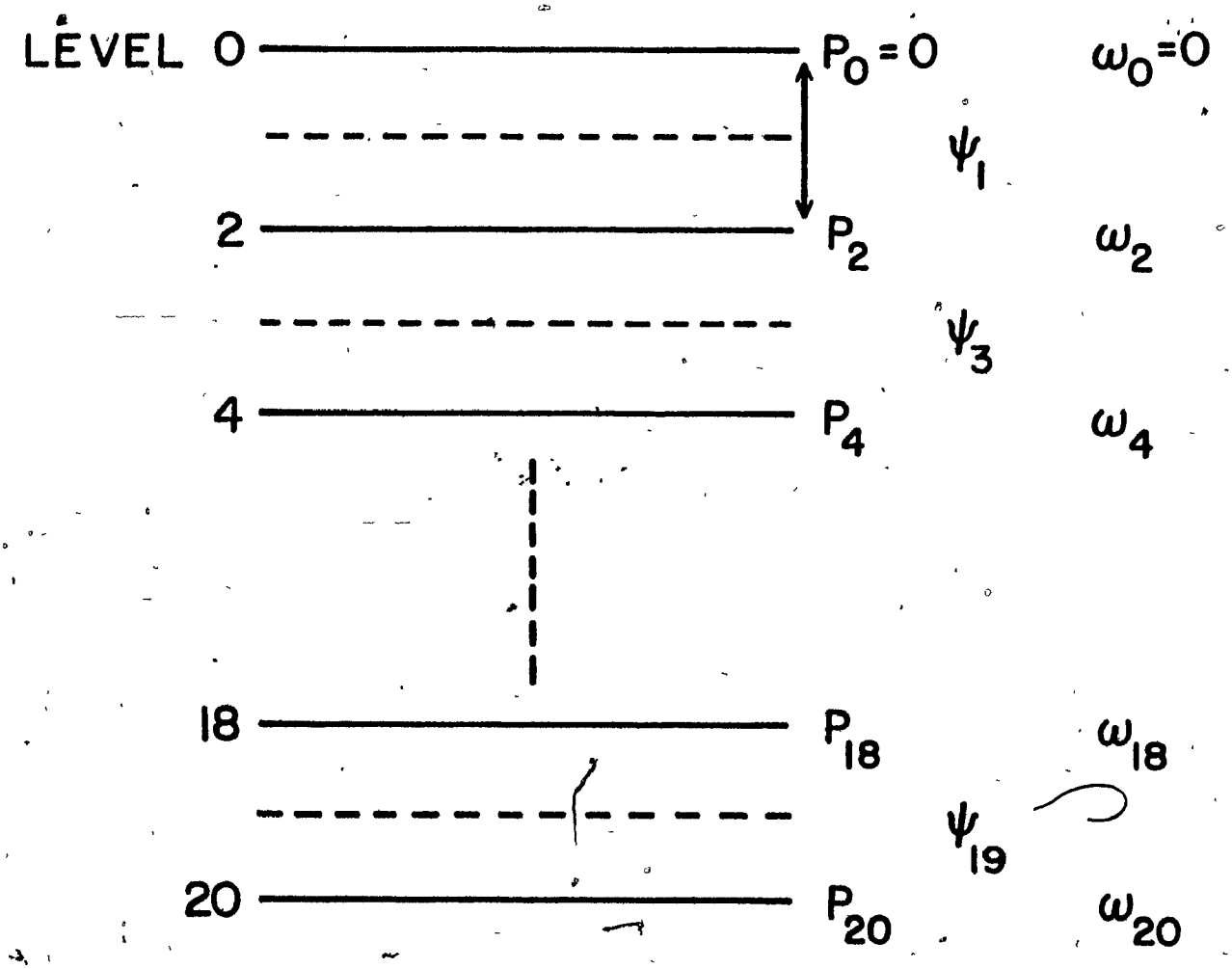

Figure 2.1 Vertical discretization of the model: p_k, Ψ_k, ω_k denote the pressure, streamfunction and pressure vertical velocity at level k.

$$q_k = \left(\nabla^2 - \mu^2_{k+1} - \mu^2_{k-1}\right) \psi_k + \mu^2_{k+1} \psi_{k+2} + \mu^2_{k-1} \psi_{k-2} + f \quad , \quad k=3,5,\cdots,17$$

$$q_{19} = \left(\nabla^2 - \mu^2_{18}\right) \psi_{19} + \mu^2_{18} \psi_{17} + f$$

$$\mu^2_{k-1} = \frac{f_o^2}{\sigma_k R \Delta p} \cdot \frac{k-1}{2} \quad , \quad \sigma_k = \left(-\frac{\partial T}{\partial p} + \frac{RT}{C_p p}\right)_k \quad , \quad k=3,5,\cdots,17$$

The total derivative d_k/dt at level k includes advection by the horizontal velocity components in the zonal (u_k) and meridional (v_k) directions; the latter velocities are given in terms of the streamfunction (ψ_k). The vertical pressure velocity $\omega_k = (dp/dt)_k$ has been eliminated to obtain (1). The other symbols σ_k, R, $\Delta p = 100$mb, T, p, C_p, ∇^2 denote the stability parameter at level k, the ideal gas constant, vertical pressure increment, temperature, pressure, specific heat at constant pressure, horizontal Laplacian, respectively. The Coriolis parameter $f = f_o + \beta y$ is assumed to be constant, except when differentiated in the meridional direction, consistent with the quasi-geostrophic β-plane approximation. The vertical boundary conditions for the inviscid analysis are vanishing vertical velocities at the top and bottom boundaries, $\omega_o = 0 = \omega_{20}$. The bottom boundary condition will be modified when surface dissipation is included later.

We use Fourier harmonics to represent variations in the horizontal. Following Lorenz (1963), we choose an appropriate set of orthogonal functions for the channel model:

$$\phi_{oj} = \sqrt{2} \cos jy_o$$

$$\phi_j = 2 \sin jy_o \cos nx_o$$

$$\phi'_j = 2 \sin jy_o \sin nx_o$$

where $x_o = x/L$ and $y_o = y/L$, with $0 \le x_o \le 2\pi$, $0 \le y_o \le \pi$; j and n are integers representing the meridional and zonal mode numbers respectively. For the most part of this study, we resolve 30 modes in the meridional direction ($1 \le j \le 30$), and the instability analysis is carried out as a function of a fixed zonal mode number (n=1,2,---). We thus do not include the subscript n in the description of the eddy modes ϕ_j, ϕ_j'. The functions (ϕ_{oj}, ϕ_j, ϕ_j') are eigenfunctions of the Laplacian operator, satisfy an orthogonality condition, and have vanishing tangential derivatives at the boundary. The Jacobian of two orthogonal functions, which arises in the advective terms, can be expressed as a series involving the complete set of orthogonal functions using interaction coefficients.

The streamfunction at each level ψ_k is expanded in a series of orthogonal functions. The boundary conditions of no normal flow at the north-south channel walls are satisfied, because of the vanishing tangential derivatives of the orthogonal functions at the walls. In the zonal direction, we assume periodic boundary conditions. The total streamfunction ψ_k consists of a basic state component ($\overline{\psi}_k$) and a perturbation component (ψ_k'):

$$\psi_k = \overline{\psi}_k + \psi_k' \tag{2a}$$

$$\overline{\psi}_k = L^2 f_o \sum_j \Psi_{kj} \phi_{oj} \qquad , \qquad U_k = -\frac{\partial \overline{\psi}_k}{\partial y} \tag{2b}$$

$$\psi_k' = L^2 f_o \, e^{\sigma t} \sum_j \left(A_{kj} \phi_j + B_{kj} \phi_j' \right) \tag{2c}$$

The streamfunction amplitudes (Ψ_{kj}, A_{kj}, B_{kj}) are all non-dimensional. The basic amplitudes Ψ_{kj} are specified using an observed Southern Hemisphere mean zonal flow (U_k) while the perturbation amplitudes (A_{kj}, B_{kj}) are calculated from the linearized version of the governing equations (1). The latter yields an eigenvalue problem for the nondimensional eigenvalue $\lambda=\sigma/f_o$, as a function of the zonal modenumber n:

$$\underset{\sim}{R}\,\underset{\sim}{X} = \lambda\,\underset{\sim}{P}\,\underset{\sim}{X} \qquad (3)$$

Here, $\underset{\sim}{R}$ and $\underset{\sim}{P}$ are square coefficient matrices, while $\underset{\sim}{X}$ is a column vector consisting of the perturbation amplitudes (A_{kj}, B_{kj}). To reduce the dimensions of the various matrices, the complex amplitude $R_{kj} = A_{kj} + iB_{kj}$ is defined for each level and each meridional mode; these then make up the vector $\underset{\sim}{X}$. The dimensions of $\underset{\sim}{R}$, $\underset{\sim}{P}$ are thus 300 x 300 (10 vertical levels, 30 meridional modes), while $\underset{\sim}{X}$ is a 300 x 1 column vector. The eigenvalue λ is found by solving (3) using IMSL computer routines. More details of the solution procedure are given in the Appendix. Instability results when the eigenvalue σ has a positive real part, implying exponential growth in time of the perturbation.

An equation for the channel averaged perturbation energy may be derived as follows:

$$\frac{\partial}{\partial t}\sum_k \left[\overline{EKE_k + EAPE_k}\right] = \sum_k \left[\overline{C_{k+1}\,(ZAPE,\ EAPE)} + \overline{C_k\,(ZKE,\ EKE)}\right] \qquad (4)$$

An overbar denotes a channel average in the zonal and meridional directions. The summation is over odd values of the pressure level index k. The perturbation energies are the eddy kinetic energy (EKE) and eddy available potential energy (EAPE). The two forms of energy conversion are the conversion of zonal available potential energy (ZAPE) to EAPE, and from

zonal kinetic energy (ZKE) to EKE. The energy and energy conversion terms at each level may be expressed as

$$EKE_k = \frac{1}{2}\left[\left(\frac{\partial \psi_k'}{\partial x}\right)^2 + \left(\frac{\partial \psi_k'}{\partial y}\right)^2\right] \tag{5a}$$

$$EAPE_k = \frac{1}{2}\,\mu_{k+1}^2\left(\psi_k' - \psi_{k+2}'\right)^2 \tag{5b}$$

$$C_{k+1}\,(ZAPE,EAPE) = \frac{1}{2}\,\mu_{k+1}^2\left(U_k - U_{k+2}\right)\left(\psi_k' - \psi_{k+2}'\right)\frac{\partial}{\partial x}\left(\psi_k' + \psi_{k+2}'\right) \tag{5c}$$

$$C_k(ZKE,EKE) = -\frac{\partial U_k}{\partial y}\,\frac{\partial \psi_k'}{\partial x}\,\frac{\partial \psi_k'}{\partial y} \tag{5d}$$

We see that the baroclinic conversion C(ZAPE,EAPE) involves the vertical shear of the mean zonal wind and the perturbation meridional heat flux. The barotropic conversion involves the horizontal mean zonal wind shear and the momentum transports (Reynolds stresses). Indeed, two useful diagnostic quantities are the heat (v'T') and momentum (u'v') transports themselves:

$$v_{k+1}'\,T_{k+1}' = \frac{f_o}{2R}\left(\psi_k' - \psi_{k+2}'\right)\frac{\partial}{\partial x}\left(\psi_k' + \psi_{k+2}'\right) \tag{6a}$$

$$u_k'\,v_k' = -\frac{\partial \psi_k'}{\partial x}\,\frac{\partial \psi_k'}{\partial y} \tag{6b}$$

Explicit expressions for the above quantities in terms of the streamfunction amplitudes (Ψ_{kj}, A_{kj}, B_{kj}) are given in the Appendix.

B. <u>The basic state</u>

The data used to obtain the basic state are the January 1979 ECMWF (European Centre for Medium Range Forecasts) level III-b FGGE (Global Weather Experiment) analyses, which are available as point values on a

1.875° by 1.875° latitude-longitude grid at 15 pressure levels from 10 mb to 1000 mb (Lambert, 1986). To obtain the mean zonal wind and temperature fields, the data were averaged over latitude circles from 20°S to 70°S, and projected onto 30 meridional Fourier harmonics, as well as the 10 pressure levels used in our model. Fig. 2.2 shows the observed zonal wind and the model wind field. We see that the meridional and vertical resolutions used produce a good approximation to the observed winds. Fig. 2.3 shows the amplitude distribution of the Fourier meridional modes of the zonal wind at 200 mb. The first mode (j = 1) has by far the largest amplitude, and the amplitudes almost vanish for mode numbers larger than 15 (j>15). The model winds are constrained to vanish at the walls at 20°S and 70°S; this distortion is not expected to have a significant effect on the instability analysis as the regions of maximum vertical and horizontal wind shears are located away from the walls. From the observed temperature field, we can calculate the static stability S at pressure level k, related to the stability parameter as follows:

$$S_k = \left[-\frac{\alpha}{\theta} \frac{\partial \theta}{\partial p} \right]_k = \frac{R}{p_k} \sigma_k$$

Here α and θ are the specific volume and potential temperature respectively. In Fig. 2.4, we show the temperature and static stability as a function of pressure at 45°S. The stability increases rapidly in the upper troposphere and lower stratosphere, as expected.

An important parameter characterizing the baroclinic instability of a zonal flow U(p) is the Richardson number, which is a measure of the relative effects of the stabilizing static stability and the destabilizing thermal wind. Following Gall (1976), we define both a conventional Richardson number (Ri) for the β-plane model, and a spherical Richardson number (Ri_s) appropriate for a sphere.

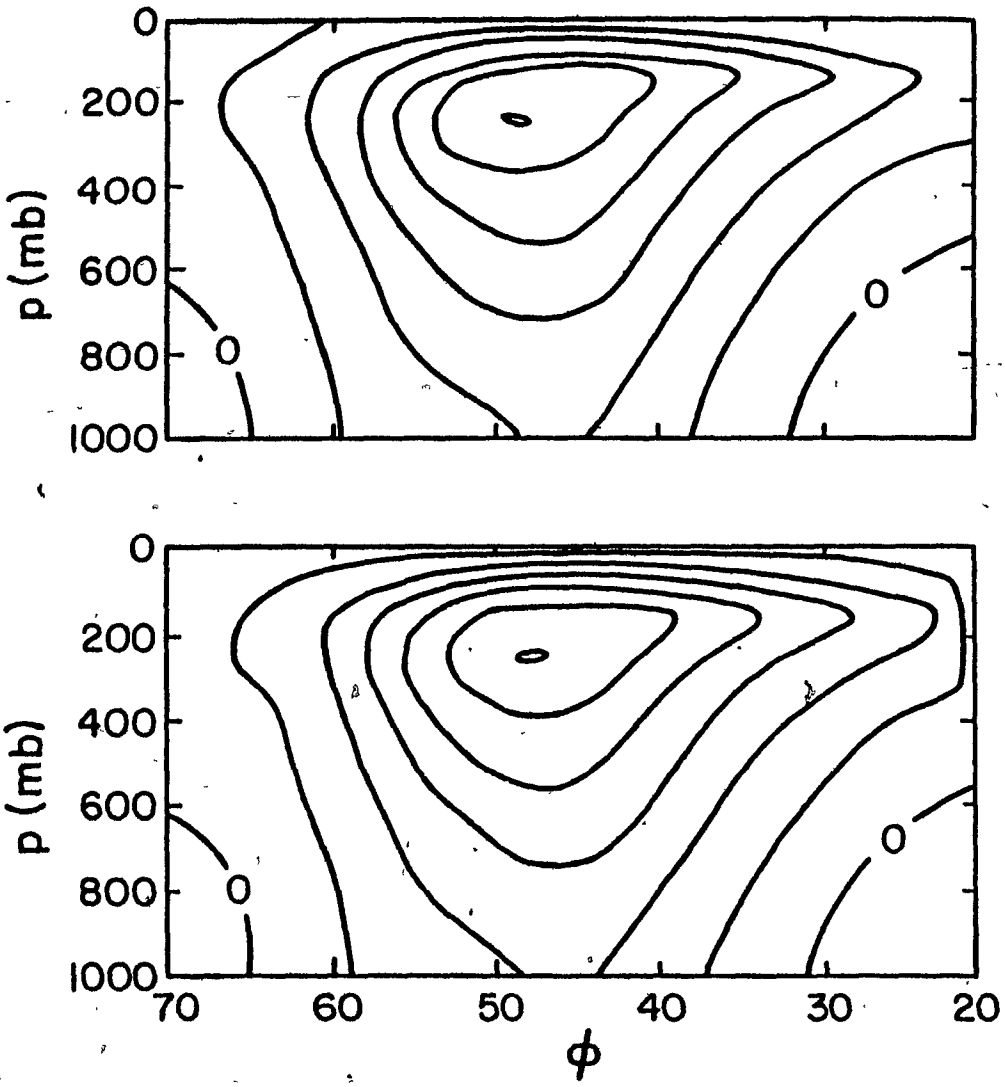

Figure 2.2 The observed (top) and model (bottom) zonal wind field as functions of pressure(p, mb) and latitude (ϕ, degree south) with 5m/s contour interval.

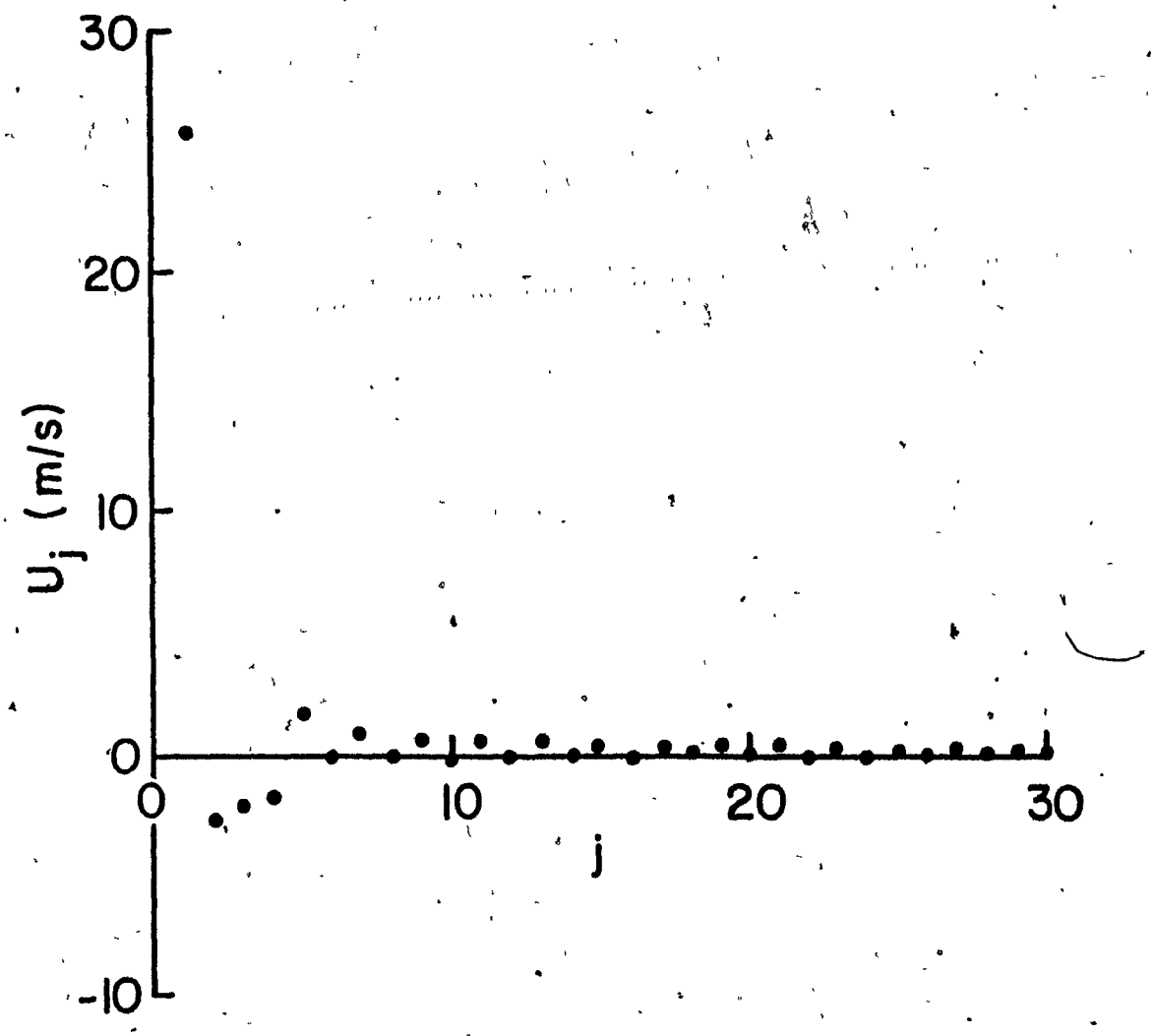

Figure 2.3 Amplitude distribution (U_j) of the 30 Fourier meridional harmonics for the zonal wind at 200mb.

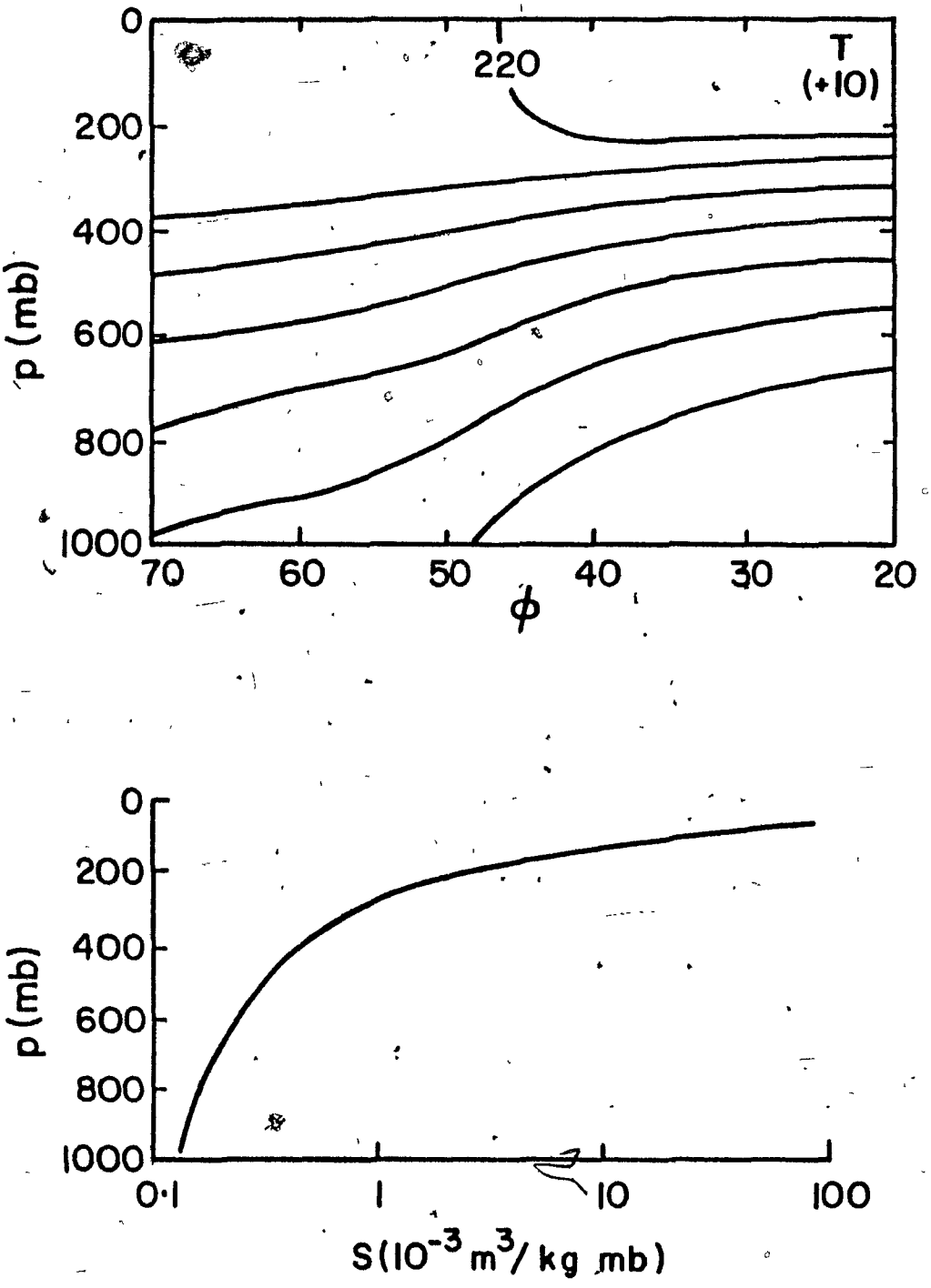

Figure 2.4 The top panel shows the basic state temperature (T) as a function of latitude (ϕ, degree south) and pressure (p, mb). The contour interval is $+10^{0}$C as indicated in brackets. The bottom panel shows the basic state static stability (S) at 45^{0}S as a function of pressure.

$$Ri = S \Big/ \left(\frac{\partial U}{\partial p}\right)^2$$

$$Ri_s = f_o^2 \, S \Big/ \left[f \frac{\partial U}{\partial p} + 2U \frac{\partial U}{\partial p} \frac{\tan \phi}{a} \right]^2$$

Here, ϕ is latitude and $f = 2\Omega \sin \phi$ is the Coriolis parameter on the sphere; Ω is the angular velocity of rotation of the earth. This modification to Ri expresses the fact that for a given vertical wind shear, the horizontal temperature gradient is larger in the north than in the south, when both points are in the same hemisphere. A second modification to Ri, motivated by the fact that solid body rotation on the sphere is the dynamical equivalence of a horizontally uniform flow on the β-plane, is given below:

$$Ri_\phi = S \Big/ \left[\frac{\partial (U/\cos\phi)}{\partial p}\right]^2$$

This modification amounts to replacing the zonal wind profile U by $U/\cos\phi$ in the definition of Ri_ϕ. Fig. 2.5 shows a comparison of the three Richardson numbers for the troposphere. The vertical resolution is not sufficient to resolve the rapidly varying static stability in the upper troposphere and lower stratosphere. The locations of minimum Richardson number are similar for all three versions, but the latitudinal extensions of relatively low values (< 60) differ for the cases, with Ri_s showing the smallest latitudinal extent. These results show that the Richardson number criterion describes similar gross characteristics for the growth of baroclinic waves in β-plane and spherical geometries. The differences, however, do imply that full spherical effects might be important.

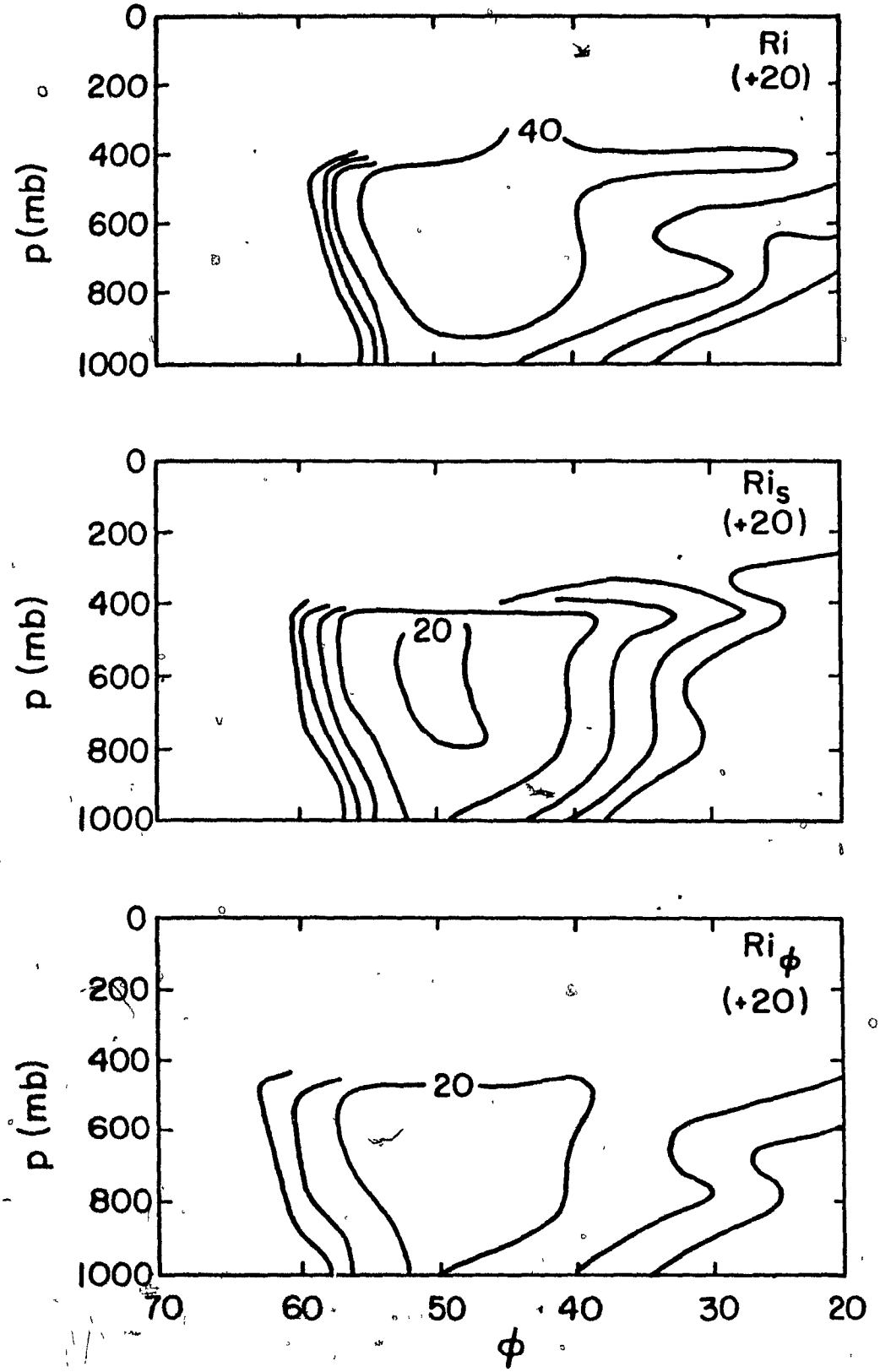

Figure 2.5 The three Richardson numbers (Ri, Ri_s, Ri_ϕ) for the troposphere, as functions of latitude (ϕ, degree south) and pressure (p, mb). The contour interval is indicated in brackets.

CHAPTER 3

Linear Instability Analysis: Part I

A. Observed and model zonal wavenumber 5 eddy structure

As discussed in the Introduction, observational evidence shows that zonal wavenumber 5 is the major component of the January 1979 eddy circulation, and that this wave might be due to baroclinic instability of the zonal mean flow. Two important eddy transports for baroclinic waves are the poleward transports of heat and momentum. In Fig. 3.1, we show latitude-pressure plots of the zonally averaged eddy kinetic energy (KE), poleward heat flux (VT) and poleward momentum flux (UV) due to zonal wavenumber 5, as obtained from the January 1979 Southern Hemisphere data set used by Lambert (1986; private communication). We see that the latitudinal structures are relatively simple: the kinetic energy peaks at about 50^{o}S while the heat and momentum transports have maxima slightly to the north. The latitudinal extent in all cases is approximatley 20^{o} latitude. The height structure shows a double maximum of comparable amplitudes in the heat transport and only a single maximum in the upper troposphere for the kinetic energy and momentum transport. These results show general agreement with the observational analysis of Chen et al. (1986), and Randel and Stanford (1985a). The latter examined the 1979/80 December-February seasonally averaged medium scale (wavenumbers 4-7) latitude-height wave structure. They found that the northward heat flux shows only a surface maximum, instead of the double maxima shown in Fig. 3.1.

We now examine the linear quasi-geostrophic instability properties of the mode corresponding to zonal wavenumber m=5 in the mid-latitude

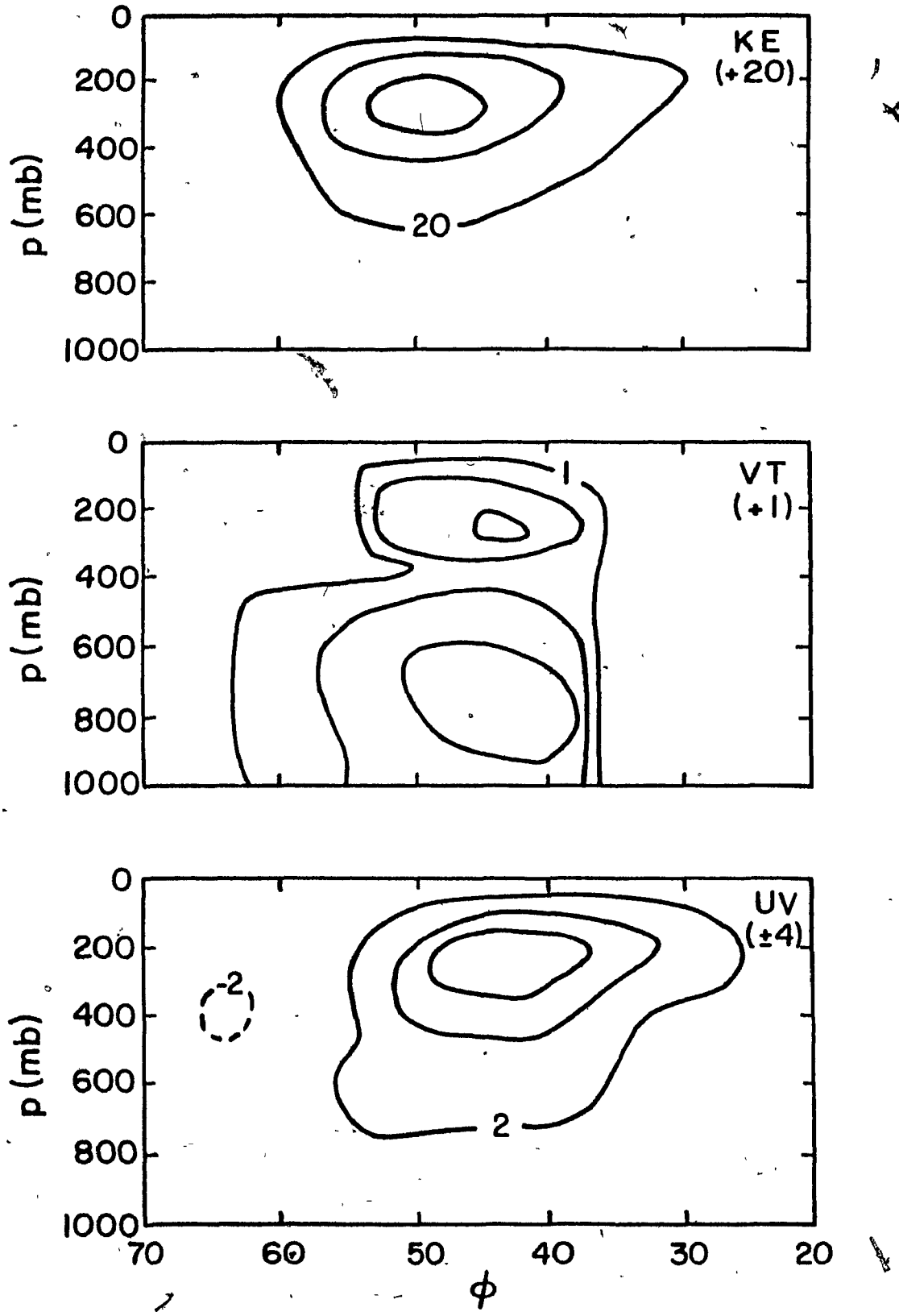

Figure 3.1 Latitude (ϕ, degree south)-pressure (p, mb) plots of the zonal wavenumber 5 kinetic energy (KE, m^2/s^2), poleward heat transport (VT, m^0 K/s) and poleward momentum transport (UV, m^2/s^2), for January 1979 Southern Hemisphere. The contour intervals are indicated in brackets. Negative contours indicate equatorward momentum transport.

Southern Hemisphere, using the basic zonal flow shown in Fig. 2.2. We first note that at ϕ_o = 45°S, the wavelength of wavenumber m = 5 is 5660 km. Because of the dimensions of the channel geometry chosen in our model, the actual zonal wavenumber (m) is related to the model zonal modenumber (n) as follows:

$$m = \frac{na\cos\phi_o}{L} = 2.54n$$

Here, a is the radius of the earth. Thus the modenumber corresponding to wavenumber 5 at 45°S is n = 2. In Fig. 3.2, we show the nondimensional growth rate, i.e. the real part of the eigenvalue (σ_r), for the unstable modes, for $1 \leq n \leq 10$. Also shown is the nondimensional frequency corresponding to eastward propagation, given by the imaginary part of the eigenvalue (σ_i). The dimensional e-folding time and period are thus $1/\sigma_r f_o$ and $2\pi/\sigma_i f_o$ respectively.

We see from Fig. 3.2 that the growth rate is maximum for mode n=5, corresponding to zonal wavenumber 12 at 45°S, with a wavelength of approximately 2400 km. The e-folding time is 2 days, typical of time scales associated with baroclinic instability. The n = 2 mode, corresponding to zonal wavenumber 5, has a smaller growth rate (e-folding time of 4 days). However, we can identify two families of unstable modes selected according to the real part of the unstable eigenvalue, i.e. the frequency. This is shown in the bottom of Fig. 3.2. Within each of the two families, the n = 2 and n = 5 modes are the most unstable mode, even though the latter mode has a larger absolute growth rate. The period of the n = 2 mode corresponding to zonal wavenumber 5 is just over 4 days; this is shorter than the observed period of about 10 days for the phase propagation of the mode.

In Fig. 3.3, we show the latitude-height sections of the structure

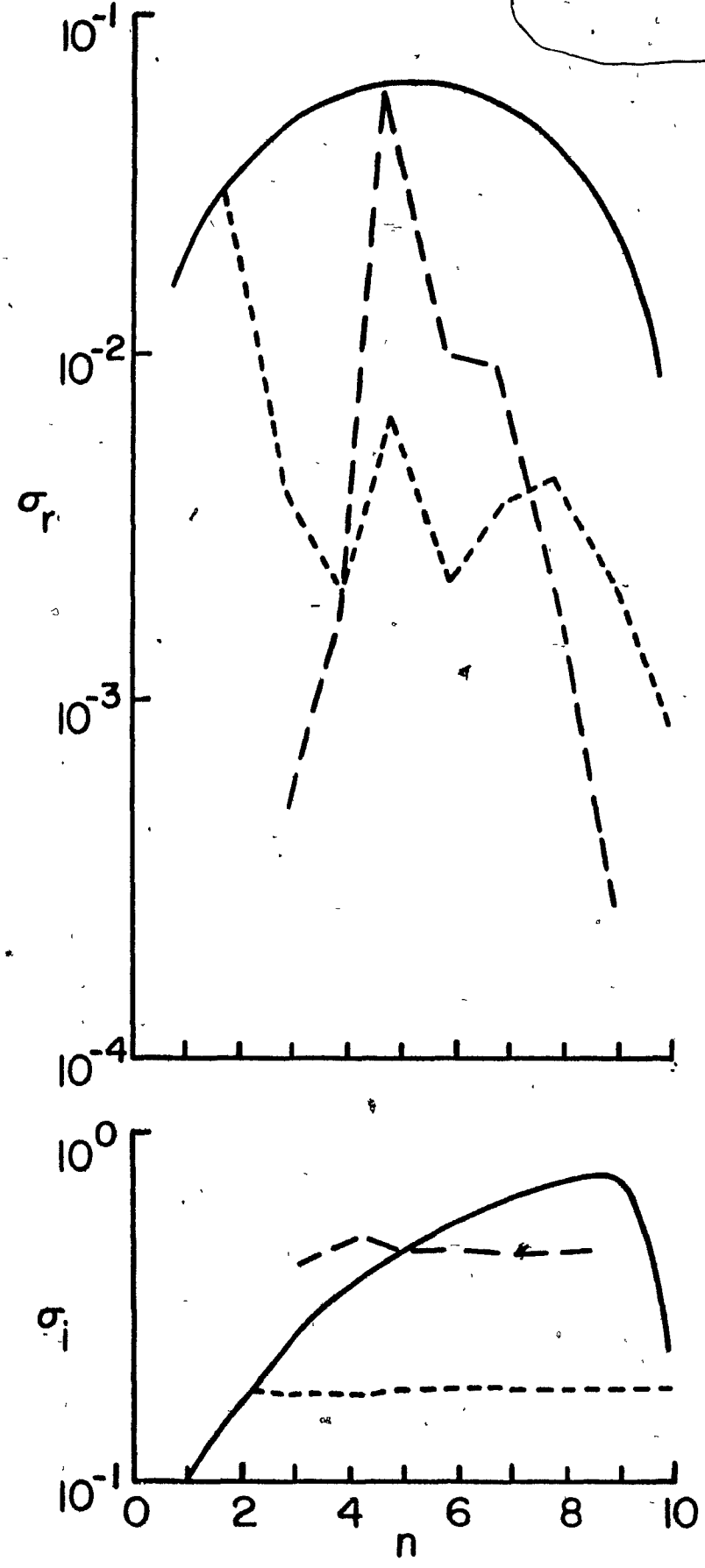

Figure 3.2 Real (σ_r) and imaginary (σ_i) parts of the unstable eigenvalue in non-dimensional units, as a function of zonal modenumber (n). The solid curve corresponds to the most unstable mode; the short and long dashed curves correspond to the families n-2 and n-5 respectively, as identifed by the real part of the eigenvalue.

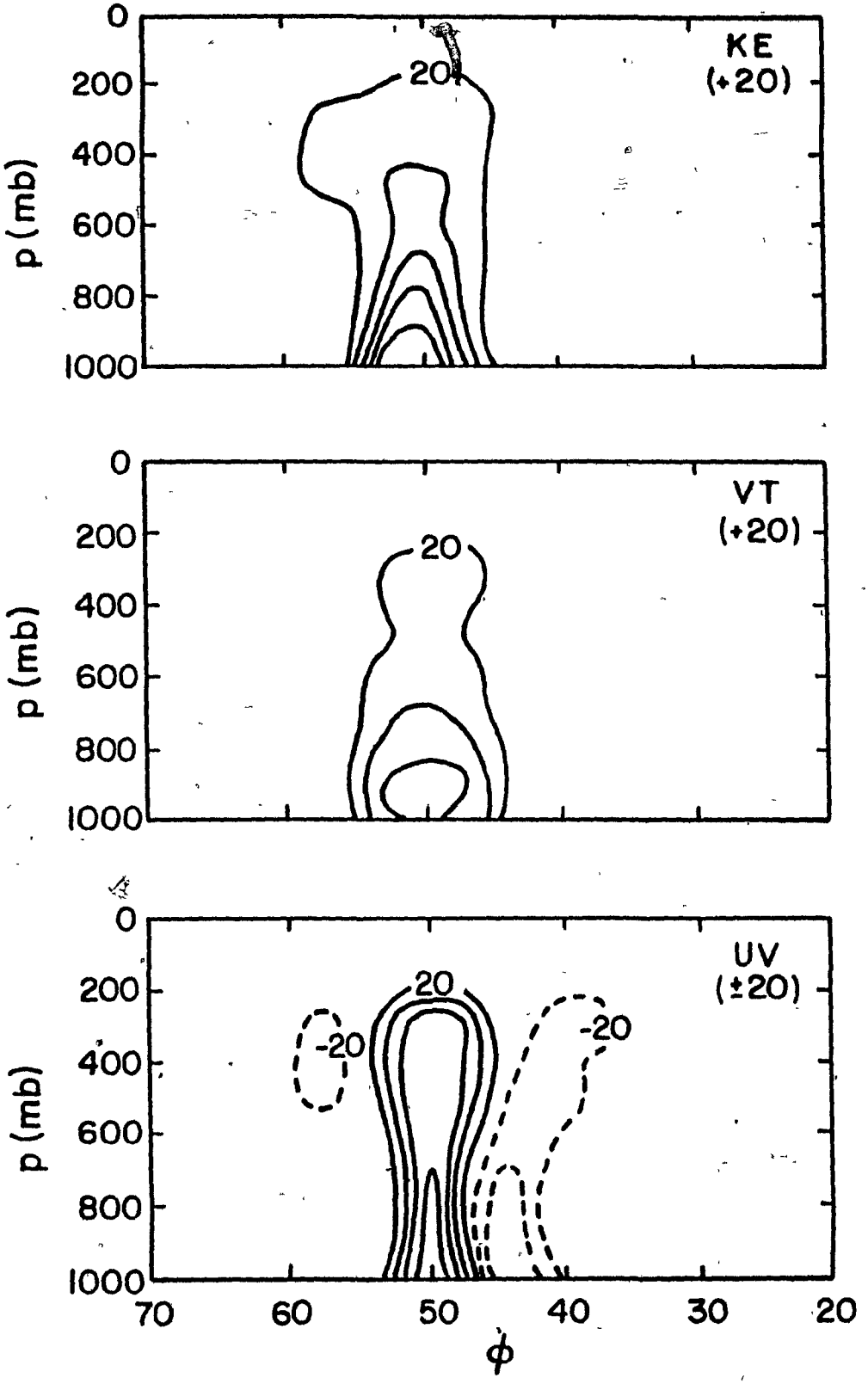

Figure 3.3 The eddy kinetic energy (KE), poleward heat transport (VT) and momentum transport (UV) as a function of latitude (ϕ, degree south) and pressure(p, mb) in arbitrary non-dimensional units for the mode n=2. The contour interval is indicated in brackets.

of the eddy kinetic energy, poleward heat and momentum transports, in arbitrary nondimensional units. The model eddy statistics all peak at the surface near 50°S, in contrast to the observed peaks in the troposphere away from the surface. This is a well known feature of linear unstable baroclinic waves (Green, 1970; Gall, 1976, Simmons and Hoskins, 1977; Frederiksen, 1981a). As a result, the double maxima in the heat transport is not simulated at all. The latitude of the maxima are reproduced, but the latitudinal extent is too small compared to observations. The regions of negative momentum transports are also exaggerated in the model results. Fig. 3.4 shows the potential energy, conversion from ZAPE to EAPE, and from ZKE to EKE, as a function of latitude and pressure. The eddy statistics are again confined to the surface near 50°S. The energy cycle is characterized by conversions from ZAPE to EAPE, and from EKE to ZKE, characteristic of baroclinic growth and barotropic conversion of baroclinically unstable waves.

B. Eddy structure of most unstable mode

We see from Fig. 3.2 that the most unstable mode occurs at n = 5, and has a zonal scale which is smaller than that of wavenumber 5. Its wavelength is about 2400 km, corresponding to wavenumber 12 at 45°S. This result has been found in earlier studies of the baroclinic instability of two-dimensional basic states (Gall, 1976; Simmons and Hoskins, 1978; Frederiksen, 1981a). These studies also show that nonlinear effects will stop the growth of these short, shallow modes, and synoptic scale modes will dominate the spectrum at that stage. The eddy structure of the mode n = 5 from the model is shown in Figs. 3.5, 3.6. The mode has maximum amplitude at about 50°S, near the surface. Its vertical scale is smaller

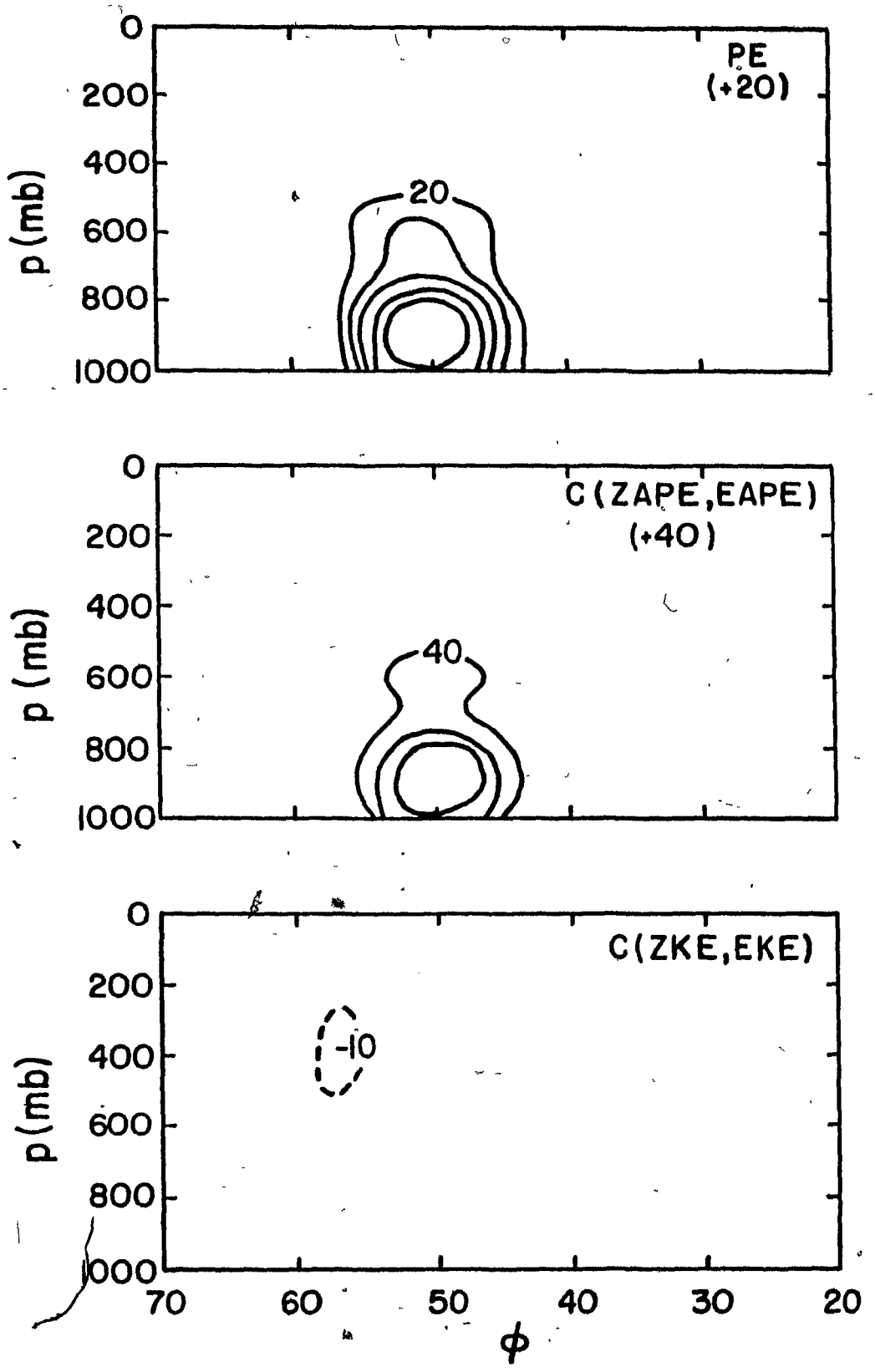

Figure 3.4 As Figure 3.3 but for the available potential energy (PE) and energy conversions C(ZAPE, EAPE), C(ZKE, EKE), for the mode n=2.

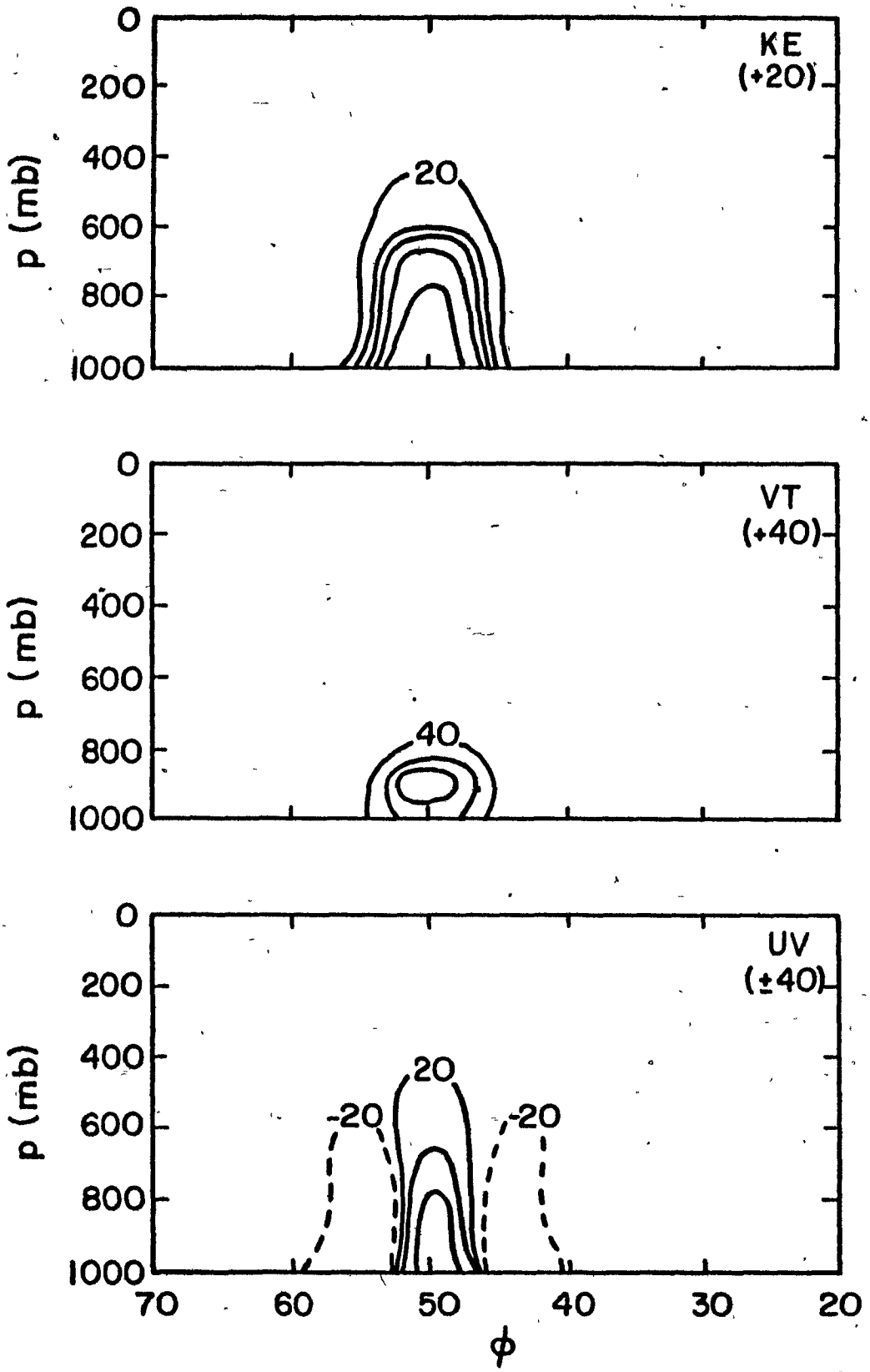

Figure 3.5 As Figure 3.3 but for the most unstable mode, n=5.

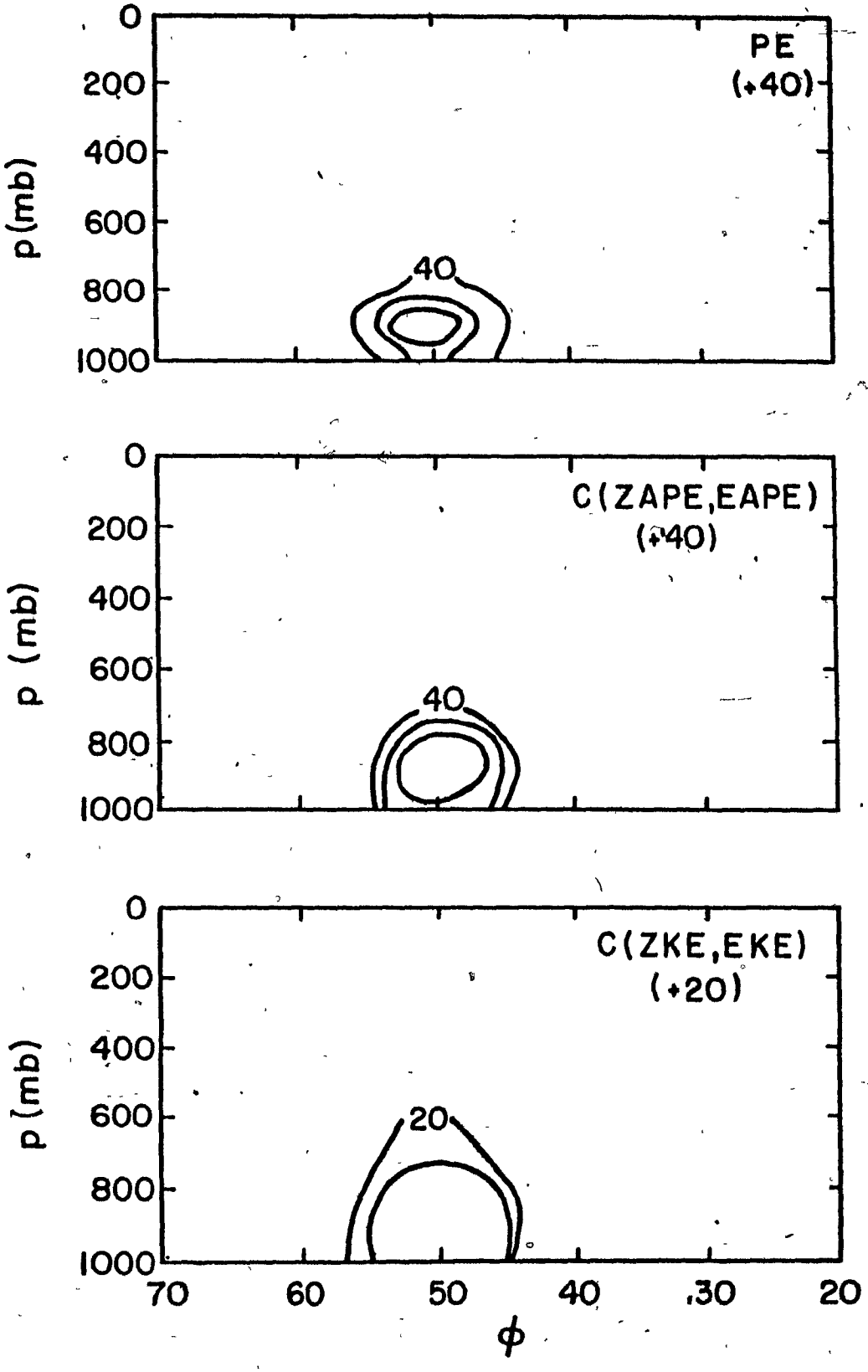

Figure 3.6 As Figure 3.4 but for the most unstable mode, n=5.

than that of the n = 2 mode examined earlier, i.e. it is a shallower mode. We also note that the energy conversion C(ZKE, EKE) is positive and has maximum amplitude near the surface, in contrast to the case of n = 2, where the conversion is negative and is largest aloft. This barotropic instability is probably due to the shallow nature of the mode. However, this barotropic conversion is small compared to the baroclinic conversion C(ZAPE, EAPE).

C. Discussion

Frederiksen (1981a) (hereafter referred to as F) has examined the instability properties of modes which grow on Southern Hemisphere zonally averaged flows for January, May and August. The January basic state was obtained from monthly averages from 1972 to 1976 as determined by the Australian Bureau of Meteorology analysis. The data set is thus not the same as that used for our basic state zonal wind. The model used by F is a linear 9-level spherical, inviscid, adiabatic quasi-geostrophic model. The vertical co-ordinate used is the σ-coordinate, i.e. pressure normalized by surface pressure. In our model, we use pressure as the vertical coordinate. Two differences between F's model and ours are thus the spherical geometry and vertical coordinate representation. F was not seeking explicitly the zonal wavenumber 5 mode, but it is instructive nonetheless to compare his results with ours.

F identified several families of unstable modes selected according to the phase speed. The most unstable mode occurs at wavenumber 10, with an e-folding time of about 2 days. This agrees with our results. The latitude-height eddy structure was shown only for the most unstable mode, which occurs at wavenumber 10, as well as for the most unstable mode at

wavenumber 4. Thus no specific attempt was made by F to examine the wavenumber 5 structure.

The zonally averaged perturbation streamfunction, temperature, momentum and heat fluxes were shown as a function of latitude and height for the most unstable mode in F. The maximum amplitudes occur at 50°S, at the surface. This agrees with our results for the n = 5 most unstable mode. Secondary maxima in the streamfunction and momentum flux were also found in the upper troposphere. F states that for wavenumber 7, the eddy statistics show more amplitude in the upper troposphere, relative to the wavenumber 10 mode, but the primary maximum still seems to be near the surface; latitude-height sections were not shown for this wavenumber.

The closest mode to the wavenumber 5 circulation that F showed is the most unstable mode at wavenumber 4. The latter has an e-folding time of about 5 days, but is a slowly westward-propagating mode; the observed wavenumber 5 circulation propagates eastward with a period of about 10 days. The maximum eddy streamfunction amplitude again occurs at the surface, but is located at 77°S. F attributed this behaviour to the fact that this mode might be propagating in the westward basic zonal flow that occurs in the stratosphere and lower troposphere between 70° and 80°S. The most unstable mode at wavenumber 4, thus bears little resemblance to the observed wavenumber 5 circulation.

We have examined the eddy structure of the n = 2 mode, which has the same wavelength as the wavenumber 5 circulation at 45°S. This mode shows a deeper vertical structure than the fastest growing n = 5 mode, with maximum eddy amplitudes at the surface near 50°S. There is, however, an indication of a secondary maximum in the upper troposphere, especially in the poleward heat and momentum fluxes (Fig. 3.3). The observed wavenumber

5 eddy statistics (Fig. 3.1) shows the primary maximum to be at about 200 mb. This vertical structure problem in linear, frictionless quasi-geostrophic baroclinic instability has already been discussed earlier. The latitudinal extent of the model n = 2 wave is too small compared to the observed circulation. We note that F found the same results for the latitudinal spread of the poleward eddy heat flux for his most unstable mode; he suggested that there might be a broadening in latitude in the nonlinear regime.

The model results so far do not show the appropriate zonal scale selection mechanism. The observed wavenumber 5 circulation frequently dominates the circulation; our results do not show this sharp scale selection in terms of growth rate. In the next section, we examine the effects of surface dissipation and a different normalization of the basic zonal wind on the scale selection.

CHAPTER 4

Linear Instability Analysis: Part II

A. Surface dissipation and normalization of zonal wind

We have seen from the results of Chapter 3 that the eddy statistics of the n = 2 wave, corresponding to zonal wavenumber 5 at 45°S, all show maximum amplitudes at the surface. The observed vertical distributions show maximum aplitudes in the upper troposphere. Here, we investigate the effects of surface dissipation, in the form of an Ekman pumping induced vertical velocity, on the perturbation vertical structure.

The surface vertical pressure velocity induced by Ekman pumping (ω_B) is

$$\omega_B = \rho f_o \frac{\partial \psi_B}{\partial t} - \rho g \left[\frac{K}{2f_o}\right]^{1/2} \nabla^2 \psi_B$$

Here, the subscript B denotes surface values; ρ, g, K are the density, gravitational acceleration and eddy viscosity respectively. In our model, the surface values are taken as $\psi_B = \psi_{19}$, $\omega_B = \omega_{20}$. In this case, the conservation of potential vorticity expressed by eqs. (1) in Chapter 2 are modified accordingly; the corresponding coefficient matrices $\underset{\sim}{R}$ and $\underset{\sim}{P}$ of eq. (3) are also changed, with $\underset{\sim}{R}$ becoming a complex matrix. The meridional resolution is reduced from 30 to 20 modes because of the extra computer storage requirements of the complex coefficient matrix. This is not expected to yield much error as the higher order modes have vanishingly small amplitudes in the basic zonal wind (Fig. 2.3). Further details are contained in the Appendix. We take two values for the eddy diffusivity, K = 5 m^2/s and K = 10 m^2/s. These values correspond to a spin down time $\tau = H(2/f_oK)^{1/2}$ of 6 and 4 days respectively for a barotropic vortex of

height H = 10 km. We will refer to these two cases as light and heavy dissipation respectively.

We show the non-dimensional growth rate (σ_r) as a function of zonal modenumber (n) in Fig. 4.1, for the cases without dissipation (a), and light (b) and heavy (c) dissipation. Case (d) will be discussed in the next section. We see that surface dissipation decreases the growth rate in all modenumbers, but does not appreciably affect the scale with the largest growth rate: the n = 5 mode remains the fastest growing mode. Thus Ekman friction is not the correct scale selection mechanism for the observed wavenumber 5 circulation. The eddy structure is shown in Figs. 4.2 and 4.3 for the light and heavy dissipation cases respectively. The two cases give similar results: a secondary maximum now appears in the kinetic energy and poleward heat transport; this maximum is of comparable magnitude as the surface maximum. The latitudinal extent of the kinetic energy aloft has increased, giving better agreement with the observed values. The latitudinal scales of the heat and momentum fluxes are still too small.

Our model is on the mid-latitude β-plane. We have so far compared the model results to the observed wavenumber 5 circulation on the sphere. To attempt to make this comparison with spherical geometry more realistic, we now divide the basic zonal wind profile by the cosine of the latitude. This normalization of the zonal wind is motivated by the fact that solid body rotation on the sphere which has a velocity profile proportional to the cosine of latitude, is dynamically equivalent to a latitudinally uniform zonal wind on the β-plane. In Fig. 4.1, we show the growth rate as a function of zonal modenumber for this case (d). We see that the growth rate of the largest scales are almost unaffected by this normalization, and that the scale of the most unstable mode occurs at n = 3, much closer to

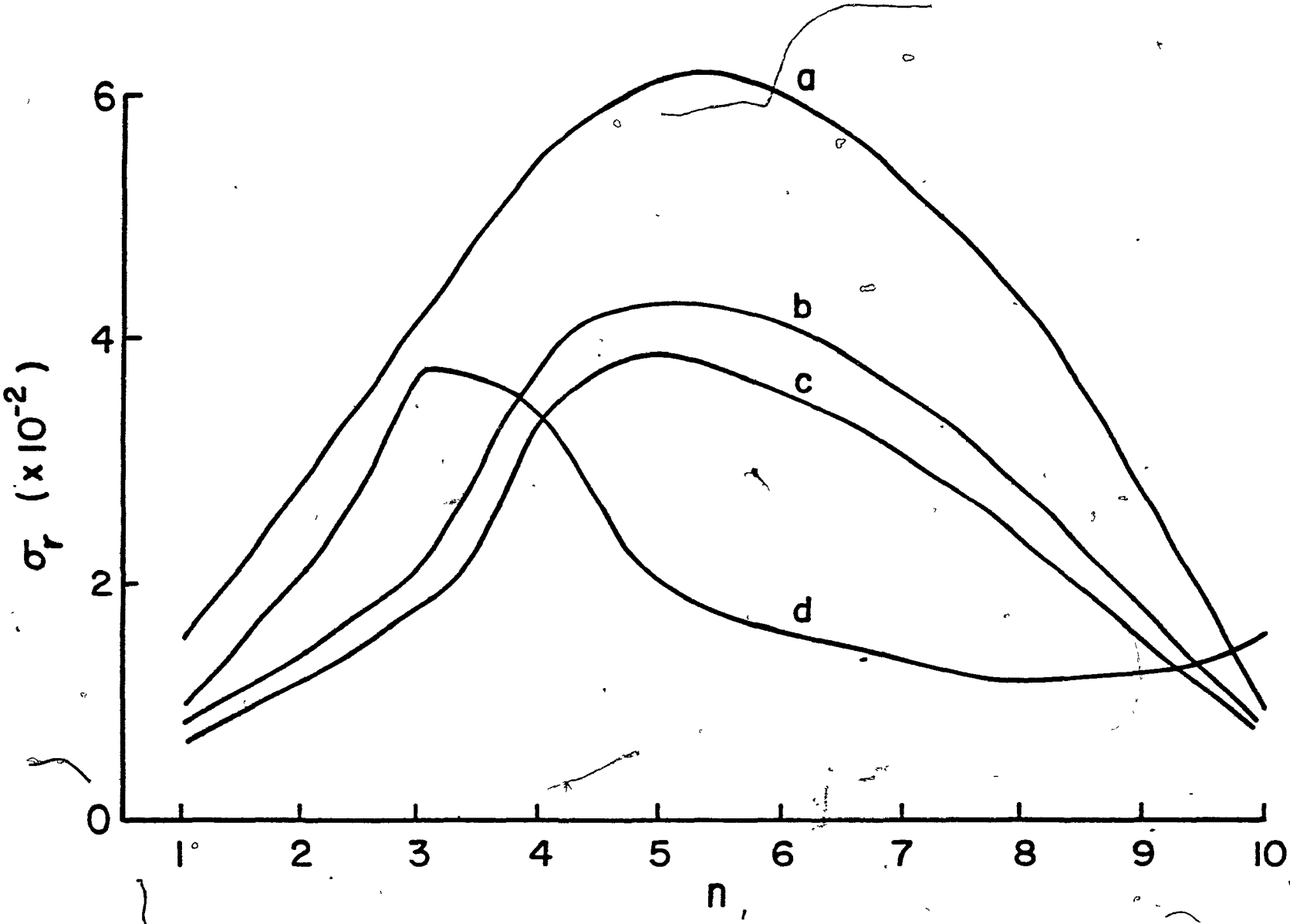

Figure 4.1 Growth rate (σ_r) in non-dimensional units as a function of zonal modenumber (n), for the cases without dissipation (a), light (b) and heavy (c) dissipation, and for zonal wind profile normalized by the cosine of latitude (d).

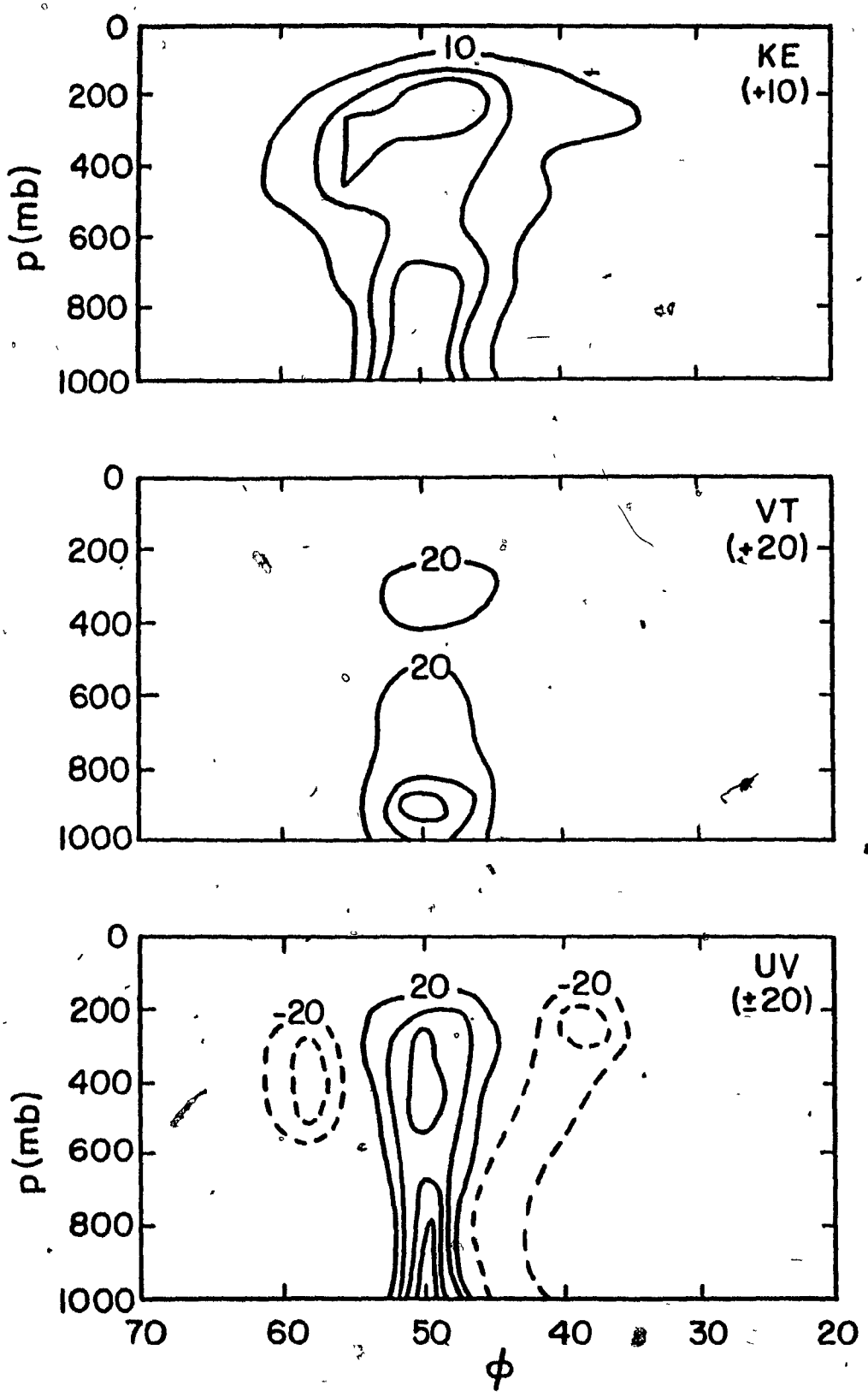

Figure 4.2 As Figure 3.3 but for the case of light dissipation.

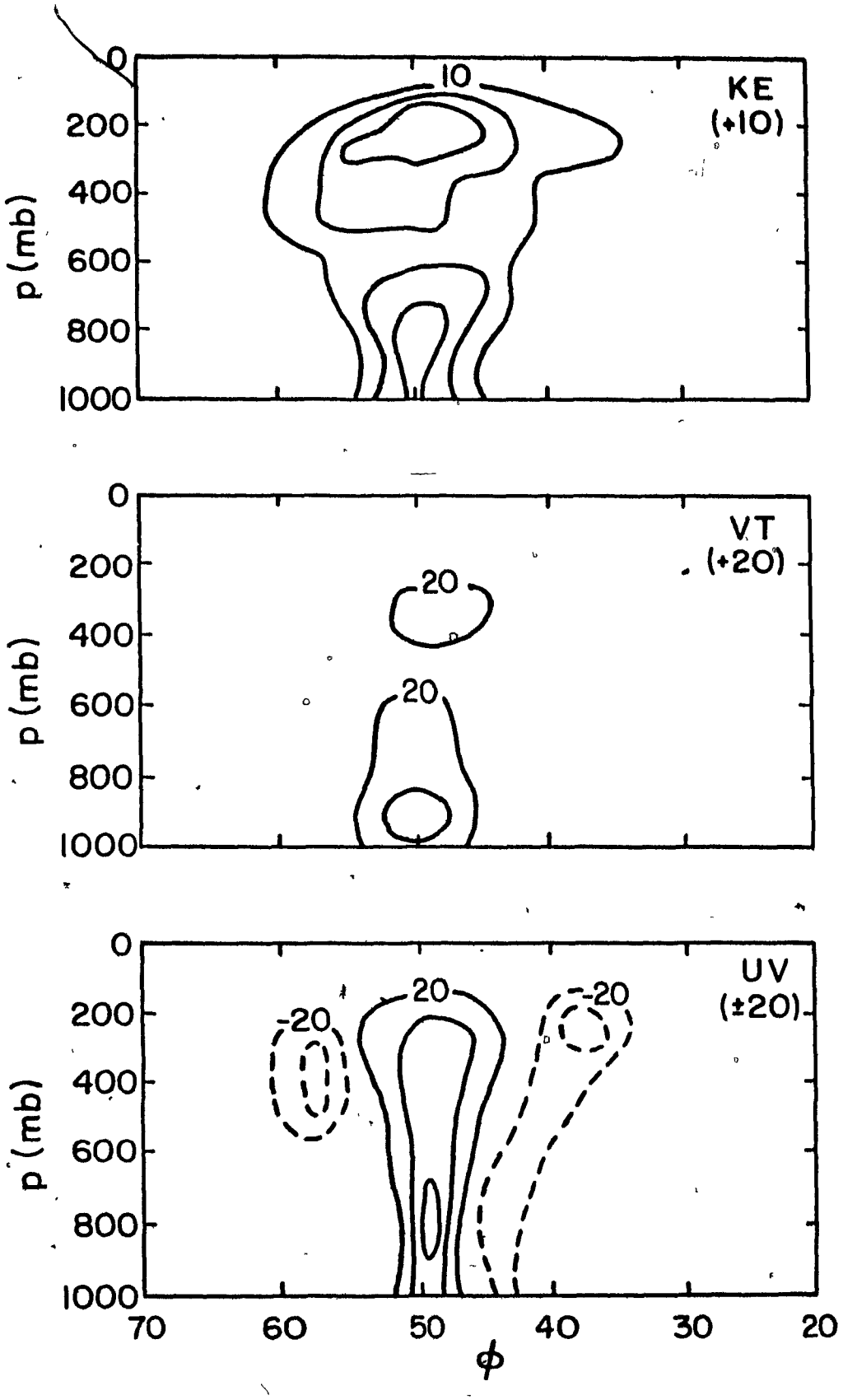

Figure 4.3 As figure 3.3 but for the case of heavy dissipation.

that of wavenumber 5 than the previous cases. Thus spherical geometry seems to be very important as a scale selection mechanism. The e-folding time (5 days) and period (3 days) of mode n = 2 corresponding to wavenumber 5 are relatively unchanged from before. Fig. 4.4 shows the eddy structure for this mode. We see that the kinetic energy now has maximum amplitude aloft, with a secondary maximum near the surface. The latitudinal position as well as the extent of the maximum are both well reproduced. However, the double maximum vertical structure of the heat transport is not reproduced here; the latitude of the maximum is also shifted slightly poleward. The momentum transport has maximum amplitude aloft, but the latitudinal position is located too far poleward and the scale is too narrow.

B. Discussion

We have examined the effects of surface dissipation and the normalization of the basic zonal wind by cosine of latitude on the eddy structure. The former is parameterized as a vertical velocity near the surface due to Ekman pumping. The latter normalization is motivated by the fact that solid body rotation on the sphere is dynamically equivalent to a latitudinally uniform wind profile. For realistic dissipative time scales corresponding to several days in the troposphere, the effects of dissipation is to reduce the growth rates for all zonal modenumbers, with no appreciable shift in the most unstable modenumber. The normalized basic wind profile gives as the most unstable mode a scale which is much closer to the observed wavenumber 5 wavelength. This suggests that spherical effects might be important for the scale selection in the Southern Hemisphere circulation.

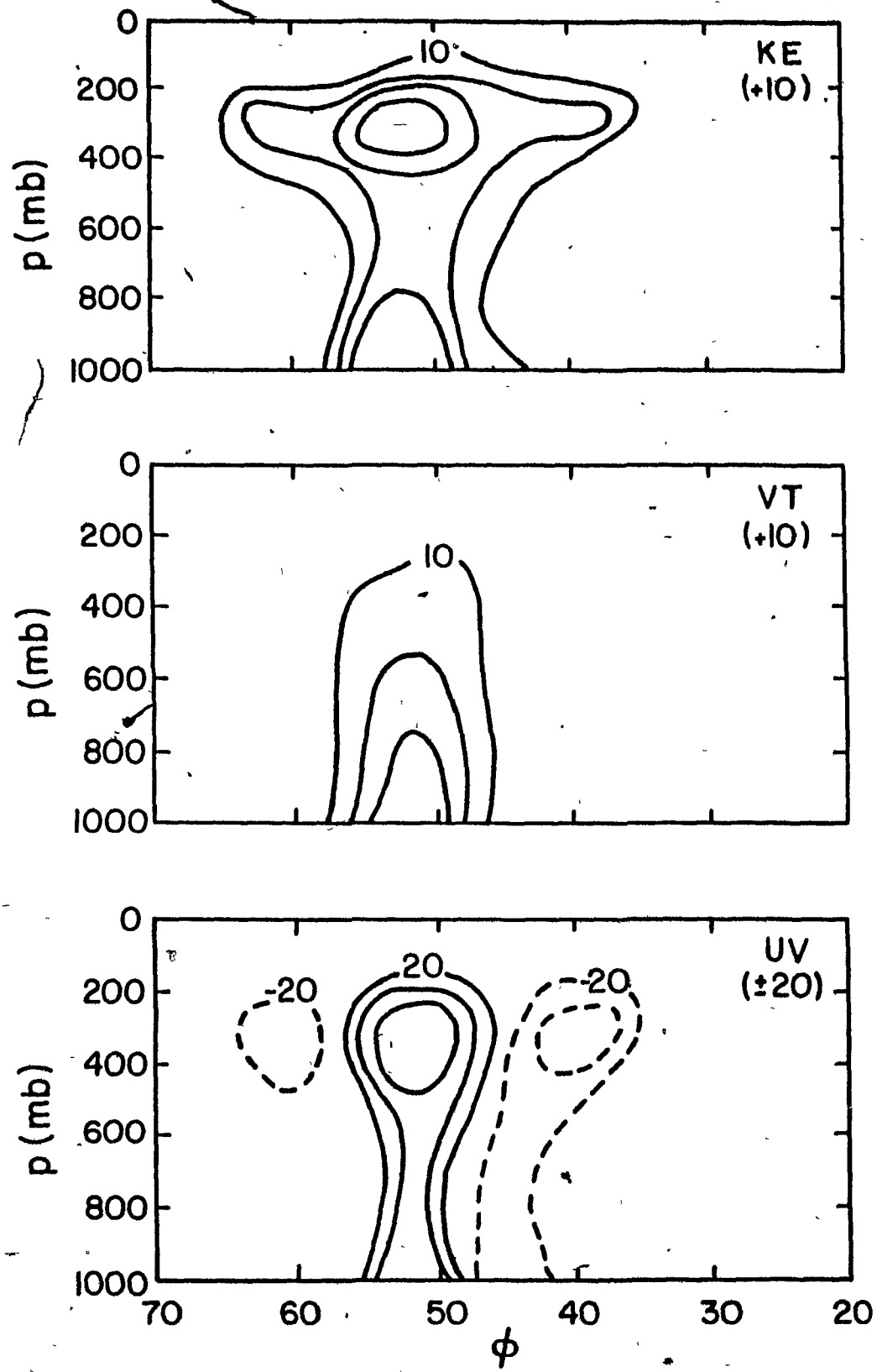

Figure 4.4 As Figure 3.3 but for the case of a zonal wind profile normalized by cosine of latitude.

The model eddy structures for the n = 2 mode show better agreement with the observed wavenumber 5 structure when surface dissipation is taken into account. In particular, the kinetic energy shows a secondary maximum aloft which is elongated in the meridional direction; the poleward heat transport also shows a seconday maximum aloft. However, the primary maximum is still near the surface. The normalized zonal wind profile gives an elongated primary maximum aloft in the eddy kinetic energy at almost the observed latitude. This is the best simulated case for the kinetic energy structure. However, the poleward heat flux does not have an amplitude maximum aloft.

The meridional momentum flux is not well modelled by any of these cases. The normalized wind yields a primary poleward flux maximum aloft and an equatorward flux to the south, in general agreement with the observed distribution. However, the poleward maximum is too narrow in latitude, while the equatorward flux is too strong. An equatorward flux to the north of the poleward maximum is also found in the model results; this feature is absent in the observed structure. However, we note that F found a very similar equatorward-poleward-equatorward momentum flux pattern in one of his linear modes - that of zonal wavenumber 10 growing on a basic state consisting of an instantaneous May 1979 zonal wind profile. He attributed this complex structure to the fact that the mode grows on both the subtropical and polar jets.

CHAPTER 5

Conclusions

We have examined the linear instability of the observed two-dimensional January 1979 zonal wind of the mid-latitude Southern Hemisphere. The motivation for doing this analysis is to investigate whether the observed Southern Hemisphere wavenumber 5 circulation is a linear baroclinically unstable mode. The model used is a 10-level, linear, quasi-geostrophic mid-latitude β-plane channel model, with 30 Fourier harmonics in the meridional direction, and a single harmonic in the zonal direction. With this horizontal and vertical resolution, the latitude-height structure of the observed zonal wind is well reproduced. The observational studies strongly suggest that the wavenumber 5 circulation is due to baroclinic instability, as it exhibits the characteristic baroclinic conversions and barotropic decay during its life cycle. The results of our study are summarized below:

(1) The most unstable mode (n=5) occurs at a zonal scale which is smaller than that of wavenumber m=5. In fact, it corresponds to wavenumber 12 at 45°S, and has an e-folding time of about 2 days. The mode with wavelength corresponding to wavenumber 5 (n=2) is also baroclinically unstable, with an e-folding time of 4 days. It is possible to identify two families of unstable modes using the phase speed given by the imaginary part of the eigenvalue, of the modes n=5 and n=2. Within each family, the modes n=5 and n=2 are the most rapidly growing. The period of the n=2 mode is 4 days, shorter than the observed period of eastward propagation of about 10 days. The latitude-height eddy structure of this mode shows

maximum amplitude near 50°S at the surface for the kinetic and potential energies, poleward heat and momentum transports. Compared to the observations of the wavenumber 5 circulation the latitudinal position is well simulated, but its extent is too small. The position is consistent with the regions of minimum Richardson number of the basic zonal flow. The observed structure also shows the maximum eddy amplitude in the upper troposphere, with a secondary maximum present in only the poleward heat flux. The energetics show typical baroclinic and barotropic conversions characteristic of baroclinic waves. The eddy structure of the most unstable mode (n=5) shows a shallower vertical structure, with maximum amplitudes again near the surface. This vertical structure problem has been discussed in the literature; it is present in models of linear baroclinic waves.

(2) Surface dissipation was introduced in an attempt to improve the vertical structure of the n=2 mode. This was modelled as a vertical velocity near the surface due to Ekman pumping, with spin-down times of the order of 4-6 days. We find that the growth rates are decreased for all modenumbers, with little change in the phase speed; the fastest growing mode is still n=5. Thus surface dissipation is not an effective scale selection mechanism. The eddy structure of the mode n=2 shows a secondary maximum in the upper troposphere of comparable amplitude to the primary maximum near the surface. The maximum aloft has an elongated latitudinal extent, in agreement with the observed structure; the double maximum in the poleward heat transport is also simulated. However, the latitudinal extent is too narrow.

We also investigated the effects of a normalization of the zonal wind by the factor cosine of latitude. This is motivated by the fact that

solid body rotation on the sphere is dynamically equivalent to a uniform latitudinal structure on the β-plane. The results show that the maximum growth rate now occurs at a zonal scale which is much closer to that of wavenumber 5 than in the previous analyses. It thus appears that spherical effects are important in the scale selection process. The eddy structure of mode n=2 reveals an elongated primary maximum in the upper troposphere at about 50°S, in good agreement with the observed results. However, the poleward heat flux once again has maximum amplitude at the surface. In all cases, the poleward momentum flux is the least well reproduced. The normalized zonal wind profile yields a maximum of this flux aloft; in all other cases, the maximum is near the surface. The latitudinal extent is too small, with the result that equatorward transports occur both to the north and south of this maximum. The equatorward transport to the south of the maximum is found in the observed transport, but with much smaller magnitude; the transport to the north of the maximum is not present in the observed values.

(3) Our results show that baroclinic instability of the observed January 1979 summer Southern Hemisphere zonal flow produces an unstable mode with qualitative resemblance to the observed wavenumber 5 circulation. However, spherical effects might be important as a scale selection mechanism for this circulation as the fastest growing mode. The latitude height eddy structure is not expected to be significantly modified by spherical geometry. Moura and Stone (1976) examined the baroclinic instability of simple two-dimensional zonal wind shear profiles on a sphere, using a linear 2-layer quasi-geostrophic model. The found that the structure of the most unstable modes are qualitatively similar to those on a β-plane. For example, the unstable waves far from neutral stability have

amplitudes which show a quasi-Gaussian behaviour with latitude on both the sphere and β-plane; this is what we found with our eddy structure on the β-plane.

Our results also show that the unstable modes have the vertical structure problem associated with linear baroclinic waves: the amplitude maximum is near the surface while observed eddy statistics indicate it should be in the upper troposphere. This has usually been attributed to nonlinear effects (Gall, 1976; Frederiksen, 1981a). We have seen that realistic surface dissipation can also improve the vertical structure in the linear regime. Frederiksen (1981b,c) has examined the nonlinear growth and vacillation cycles of waves in Southern Hemisphere zonal flows with a multi-level spherical model. He finds that zonal wavenumber 7 is the dominant wavenumber with amplitude maximum in the upper troposphere, at the first peak in the vacillation cycle. The initial zonal flow that he used is the January zonal mean flow profile obtained from 1972-76 monthly averages from the Australian Bureau of Meteorology analysis. Hamilton (1983) examined the Australian data and found a prominent wavenumber 5 circulation during over one-quarter of the summer months from November through March, 1972-1979. The dominance of this wavenumber was first discussed by Salby (1982). Thus Frederiksen was probably not aware of its importance at the time of his study. His use of the monthly average January zonal flow from 1972 to 1976 might also have somewhat masked the dominance of this wavenumber. It would be of great interest to first repeat the present analysis with spherical geometry and surface dissipation with the observed January 1979 zonal flow, and then to perform a nonlinear initial value analysis using the observed zonal flow and the most unstable mode is initial conditions. The results would show the potential importance of spherical effects and nonlinearity in the selection and maintenance of the wavenumber 5 circulation.

Appendix

The set of linear algebraic equations (3) for the non-dimensional growth rate $\lambda = \sigma/f_0$ may be obtained from the linearized governing equations (1). The linearization is around the basic state zonal flow described by equation (2b); the perturbations consist of the eddy modes described by equation (2c). The streamfunction amplitudes of the zonal flow (Ψ_{kj}) and of the perturbations (A_{kj}, B_{kj}) are all non-dimensional. We form the complex eddy amplitude R_{kj} at vertical level k for meridional harmonic j :

$$R_{kj} = A_{kj} + iB_{kj}$$

Substituting the Fourier expansions (2b),(2c) into the linearized version of the governing equations (1), we project all terms into the set of basic functions truncated at the first 30 meridional harmonics. Replacing the eigenvalue σ by $-i\sigma$, we then get a set of real coupled linear algebraic equations for the non-dimensioned eigenvalue $-i\sigma/f_0$, and the eigenvectors consisting of the eddy amplitudes (A_{kj}, B_{kj}), for the top level (k = 1), intermediate levels (k = 3, 5,.....17) and the bottom level (k = 19);these equations are given below.

k = 1 :

$$\left[-\frac{i\sigma}{f_0}\right]\left[-\left(n^2+j^2+r_2^2\right)R_{1j} + r_2^2 R_{3j}\right]$$

$$-\sum_{p,q}\left\{\left[\left(p^2-q^2-n^2\right)\Psi_{1p} - r_2^2\Psi_{3p}\right] C_{pjq}R_{1q} + r_2^2 C_{pjq}\Psi_{1p}R_{3q}\right\} - n\frac{\beta L}{f_0}R_{1j} \qquad \text{(A1)}$$

$k = 3, 5, \ldots\ldots 17$:

$$\left(-\frac{i\sigma}{f_0}\right)\left[-(n^2+j^2+r_{k+1}^2+r_{k-1}^2)R_{kj}+r_{k+1}^2R_{k+2,j}+r_{k-1}^2R_{k-2,j}\right]$$

$$-\sum_{p,q}\Big\{\left[(p^2-q^2-n^2)\Psi_{kp}-r_{k+1}^2\Psi_{k+2,p}-r_{k-1}^2\Psi_{k-2,p}\right]C_{pjq}R_{kp}$$

$$+r_{k+1}^2C_{pjq}\Psi_{kp}R_{k+2,q}+r_{k-1}^2\Psi_{kp}C_{pjq}R_{k-2,q}\Big\}-n\frac{\beta L}{f_0}R_{kj} \qquad (A2)$$

$k = 19$:

$$\left(-\frac{i\sigma}{f_0}\right)\left[-(n^2+j^2+r_{18}^2)R_{19,j}+r_{18}^2R_{17,j}\right]$$

$$-\sum_{p,q}\Big\{\left[(p^2-q^2-n^2)\Psi_{19,p}-r_{18}^2\Psi_{17,p}\right]C_{pjq}R_{19,q}+r_{18}^2C_{pjq}\Psi_{19,p}R_{17,q}\Big\}-n\frac{\beta L}{f_0}R_{19,j} \qquad (A3)$$

Here, $r_{k-1}^2=\mu_{k-1}^2L^2$, $(k=3,5,\ldots 19)$ is the non-dimensional value of μ_{k-1}^2 and the interaction coefficients C_{pjq} are given by

$$C_{pjq} = 0 \qquad (p+j+q \text{ even})$$

$$C_{pjq} = -\frac{8/2}{\pi}njqp^2\left[\frac{(p+j+q)}{(-p+j+q)}\frac{(p-j+q)}{(p+j-q)}\right] \qquad (p+j+q \text{ odd})$$

The summations extend over the range $1 \leq p,q \leq 30$, for the case of 30 Fourier harmonics. The coefficient matrices $\underset{\sim}{R}$ and $\underset{\sim}{P}$ may be read off from the above equations after defining the eigenvector consisting of the set of complex amplitudes $\{ R_{kj} \}$.

The expressions in terms of the eddy amplitudes (A_{k_j}, B_{kj}) for the various perturbations energies and energy conversions in equations (5) and (6) at time $t = 0$ are given below.

$$EKE_k = 2 L^2 f_0^2 \sum_{p,q} (n^2+pq) \sin py_0 \sin qy_0 (A_{kp}A_{kq} + B_{kp}B_{kq})$$

$$EAPE_{k+1} = L^2 f_0^2 r_{k+1}^2 \sum_{p,q} \sin py_0 \sin qy_0 \left[(A_{kp} - A_{k+2,p}) (A_{kp} - A_{k+2,q}) \right.$$

$$\left. + (B_{kp} - B_{k+2,p}) (B_{kp} - B_{k+2,q}) \right]$$

$$C_{k+1}(ZAPE,EAPE) = \sqrt{2}\, L^2 f_0^3 n\, r_{k+1}^2 \sum_{pjq} p \sin py_0 \sin jy_0 \sin qy_0 (\Psi_{kp} - \Psi_{k+2,p})$$

$$\left[(B_{kj} + B_{k+2,j})(A_{kq} - A_{k+2,q}) - (A_{kj} + A_{k+2,j})(B_{kq} - B_{k+2,q}) \right]$$

$$C_k(ZKE,EKE) = 2\sqrt{2}\, L^2 f_0^3 n \sum_{pjq} p^2 q \cos py_0 \sin jy_0 \sin qy_0\, \Psi_{kp} (B_{kj}A_{kq} - A_{kj}B_{kq})$$

$$V'_{k+1}T'_{k+1} - 2\,L^3 f_0^2 n \sum_{p,q}^{-} \sin py_0 \sin qy_0 \Big[(B_{kp} + B_{k+2,p})(A_{kq} - A_{k+2,q})$$

$$- (A_{kp} + A_{k+2,p})(B_{kq} - B_{k+2,q}) \Big]$$

$$U'_k V'_k = -2\,L^2 f_0^2 n \sum_{p,q}^{-} p \sin py_0 \sin qy_0 \,(A_{kp}B_{kq} - B_{kp}A_{kq})$$

With the inclusion of surface dissipation as modelled by an Ekman pumping vertical velocity, the equation (A3) for the lowest level (k = 19) streamfunction amplitude is modified :

k = 19 :

$$\left(-\frac{i\sigma}{f_0}\right)\left[-\left(n^2+j^2+r_{19}^2 + \rho\frac{f_0 L^2}{\Delta p}\right) R_{19,j} + r_{18}^2 R_{17,j}\right]$$

$$-\sum_{p,q}^{-}\left\{\left[(p^2-q^2-n^2)\Psi_{19,p} - r_{18}^2\Psi_{17,p}\right] C_{pjq} R_{19,q} + r_{18}^2 C_{pjq}\Psi_{19,p} R_{17,q}\right\}$$

$$- n\frac{\beta L}{f_0} R_{19,j} + i\frac{\rho g}{\Delta p}\left(\frac{K}{2f_0}\right)^{1/2}(n^2+j^2)\,R_{19,j}$$

REFERENCES

Brown, J. A., 1969 : A numerical investigation of hydrodynamic instability and energy conversions in the quasi-geostrophic atmosphere. Part I and Part II. J.Atmos.Sci. 26, 352-365 and 366-375.

Charney, J.G., 1947 : The dynamics of long waves in a baroclinic westerly current. J.Meteor. 4, 135-163.

Chen, T. C., M. C. Yen and D. P. Nune, 1986. : Dynamic aspects of the southern-hemisphere medium-scale waves during the summer season. Extended abstract, Second international conference on southern hemisphere meteorology, Wellington, New England.

Eady, E. T., 1949 : Long waves and cyclone waves. Tellus 1, 33-52.

Frederiksen, J. S., 1978 : Growth rates and phase speeds of baroclinic waves in multi-level models on a sphere. J.Atmos.Sci. 35, 1816-1826.

——, 1981a : Disturbances and eddy fluxes in southern hemisphere flows: Linear theory. J.Atmos.Sci. 38, 673-689.

——, 1981b : Growth and vacillation cycles of disturbances in southern hemisphere flows. J.Atmos.Sci. 38, 1360-1375.

——, 1981c : Scale selection and energy spectra of disturbances in southern hemisphere flows. J.Atmos.Sci. 38, 2573-2584.

Gall, R., 1976a : A comparison of linear baroclinic instability theory with the eddy statistics of a general circulation model. J.Atmos.Sci. 33, 349-373.

——, 1976b : Structural changes of growing baroclinic waves. J.Atmos.Sci. 33, 374-390.

Green, J. S. A., 1970 : Transfer properties of large-scale eddies and the general circulation of the atmosphere. Quart. J. Roy. Meteor. Soc. 96, 157-184.

Hamilton, K., 1982 : Aspects of wave behaviour in the mid- and upper troposphere of the southern hemisphere. Atmos.-Ocean 21(1), 40-54.

Kalnay, E., K. C. Mo and J. Paegle, 1986 : Large-amplitude, short-scale stationary Rossy waves in the southern hemisphere : Observations and mechanistic experiments to determine their origin. J.Atmos.Sci. 43, 252-275.

Lambert, S. J., 1986 : A study of the eddy kinetic energy of the southern hemisphere during January and July with emphasis on the FGGE year. Tellus 38A, 429-438.

Lin, C. A., 1982 : The effects of latitudinal asymmetries on baroclinic instability. Atmos.-Ocean 20(2), 143-157.

Lorenz, E. N., 1963 : The mechanics of oscillation. J.Atmos.Sci. 20, 448-464.

Moura A. D. and P. H. Stone 1976 : The effects of spherical geometry on baroclinic instability. J.Atmos.Sci. 33, 602-616.

Randel, W. J. and J. L. Stanford, 1983 : Structure of medium-scale atmospheric waves in the southern hemisphere summer. J.Atmos.Sci. 40, 2312-2318.

——, and ——, 1985a : An observational study of medium-scale wave dynamics in the southern hemisphere summer. Part I : Wave structure and energetics. J.Atmos.Sci. 42, 1172-1188.

——, and ——, 1985b : An observational study of medium-scale wave dynamics in the southern hemisphere summer. Part II : Stationary-transient wave interference. J.Atmos.Sci. 42, 1189-1197.

——, and ——, 1985c : The observed life cycle of a baroclinic instability. J.Atmos.Sci. 42, 1364-1373.

Schoeberl, M. R. and A. J. Krueger, 1983 : Medium scale disturbances in total ozone during southern hemisphere summer. Bulletin Amer.Meteor.Soc. 29, 38-52.

Simons, T. J., 1971 : The nonlinear dynamics of cyclone waves. J.Atmos.Sci. 29, 38-52.

Simmons, A. J. and B. J. Hoskins, 1977 : Baroclinic instability on the sphere: solution with a more realistic tropopause. J.Atmos.Sci. 34, 581-588.

——, and ——, 1978 : The life cycles of some nonlinear baroclinic waves. J.Atmos.Sci. 35, 414-432.

Song, R. T., 1971 : A numerical study of the three-dimensional structure and energetics of unstable disturbances in zonal currents : Part I and Part II. J.Atmos.Sci. 28, 549-564 and 565-586.